

Evaluation of brain ischemia/reperfusion injury and the impact of new neuroprotective strategies using Magnetic Resonance Imaging



Máster en Física Médica

Facultad de Ciencias

Agustín Clemente Moragón

Centro Nacional de Investigaciones Cardiovasculares (CNIC)

Tutora UNED: Cristina Santa Marta Pastrana

Tutor CNIC: Borja Ibáñez Cabeza

Junio 2023

ÍNDICE

ABBREVIATIONS.....	3
ABSTRACT.....	4
RESUMEN.....	4
GENERAL INTRODUCTION.....	5
Ischemic stroke.....	6
Magnetic Resonance Imaging.....	6
Imaging in ischemic stroke.....	9
Beta-adrenergic receptors and beta-blockers.....	10
Cardioprotective effect of metoprolol on AMI.....	10
Neutrophils, Ischemia/Reperfusion Injury and metoprolol.....	11
OBJECTIVES.....	13
MATERIAL AND METHODS.....	15
Animals.....	16
Rat procedures.....	16
Cerebral ischemia-reperfusion injury.....	16
Brain magnetic resonance imaging.....	17
Infarct size and oedema quantification.....	18
Rat carotid artery catheterization and hemodynamic dose-response characterization.....	19
Tissue processing.....	19
Rat brain staining and quantification.....	19
Statistics.....	21
RESULTS.....	22
Selective ADRB1 blockade during ongoing stroke reduces brain injury, prevents neuronal loss and improves neurological outcomes.....	23
ADRB1 blockade reduces brain cytotoxic and vasogenic oedema.....	26
ADRB1 blockade preserves BBB integrity.....	27
ADRB1 blockade during brain ischemia prevents microglia/macrophage response and reduces sub-acute glial scar formation.....	29
DISCUSSION.....	32
CONCLUSIONS.....	36
Author contributions.....	38

Acknowledgements	38
Funding	38
BIBLIOGRAPHY	40
APPENDIX	45

ABBREVIATIONS

Abbreviations	Meaning
AAR	Area-at-risk
ADC	Apparent diffusion coefficient
ADRB	Beta adrenergic receptor
AQP4	Aquaporin-4
AMI	Acute myocardial infarction
BBB	Blood brain barrier
BP	Blood pressure
CMR	Cardiac magnetic resonance
CSPG	Chondroitin sulfate proteoglycan
CT	Computerized tomography
DCE	Dynamic contrast-enhanced
DSC	Dynamic susceptibility contrast
DWI	Diffusion-weighted image
ECV	Extracellular volume
GFAP	Glial fibrillary acidic protein
GPCR	G-protein coupled receptor
GRE	Gradient echo
HT	Hemorrhagic transformation
HR	Heart rate
Iba1	Ionized calcium-binding adapter molecule 1
IRI	Ischaemia-reperfusion injury
IHC	Immunohistochemistry
IF	Immunofluorescence
I/R	Ischemia/Reperfusion
IS	Infarct size
i.v.	Intravenous
FID	Free induction decay
MBP	Myelin basic protein
MCA	Middle cerebral artery
MCAO/R	Middle cerebral artery occlusion/reperfusion
MVO	Microvascular obstruction
MRI	Magnetic resonance imaging
NeuN	Neuronal nuclear marker
PCI	Percutaneous coronary intervention
PDM	Perfusion-diffusion mismatch
RF	Radiofrequency
ROI	Region of interest
rt-PA	Recombinant tissue plasminogen activator
SE	Spin echo
STEMI	ST-elevation myocardial infarction
TE	Echo time
TR	Repetition time
T1W	T1 weighted
T2W	T2 weighted
B₀	External magnetic field

ABSTRACT

Reperfusion therapy is the standard of care for ischemic stroke; however, there is a need to identify new therapeutic targets able to ameliorate cerebral damage. Neutrophil β 1-adrenergic receptors (ADRB1) have been linked to neutrophil migration during exacerbated inflammation. Given the central role of neutrophils in cerebral damage during stroke, we hypothesize that ADRB1 blockade will improve stroke outcomes. For this purpose, young adult male Wistar rats were subjected to middle cerebral artery occlusion–reperfusion to evaluate the effect on stroke of the selective ADRB1 blocker metoprolol (12.5 mg/kg) when injected intravenously (i.v.) 10 min before reperfusion. Magnetic resonance imaging (MRI) at 24 h and 7 d, as well as histopathology analysis, showed that pre-reperfusion i.v. metoprolol reduced infarct size and exerted a neuroprotective effect. Besides, MRI results revealed that this effect was accompanied by reduced cytotoxic and vasogenic oedema at 24 h and 7 d, respectively. Attenuation of vasogenic oedema was consistent with a better preservation of blood-brain barrier integrity at 7 d post-reperfusion. To conclude, our findings describe that ADRB1 blockade ameliorates cerebral damage, thus identifying a novel therapeutic target to improve outcomes in patients with stroke. This therapeutic strategy is in the earliest stages of the translational pathway and should be further explored.

RESUMEN

La terapia de reperfusión es el tratamiento estándar para el accidente cerebrovascular isquémico; sin embargo, existe la necesidad de identificar nuevas dianas terapéuticas capaces de mejorar el daño cerebral. Los receptores β 1-adrenérgicos (ADRB1) expresados en la superficie del neutrófilo se han relacionado con la migración de neutrófilos durante la inflamación exacerbada. Dado su papel central en el daño cerebral durante un accidente cerebrovascular, planteamos la hipótesis de que el bloqueo de ADRB1 supondría una mejoría en este contexto. Para ello, ratas Wistar adultas jóvenes se sometieron a un modelo de oclusión-reperfusión de la arteria cerebral media para evaluar el efecto del bloqueador selectivo ADRB1 metoprolol (12.5 mg/kg) sobre el accidente cerebrovascular tras su administración por vía intravenosa (i.v.) 10 min antes de la reperfusión. La resonancia magnética nuclear a las 24 h y 7 d, así como el análisis histopatológico, mostraron que la administración i.v. pre-reperfusión de metoprolol fue capaz de reducir el tamaño del infarto y ejercer un efecto neuroprotector. Este efecto se acompañó de una reducción del edema citotóxico y vasogénico a las 24 h y 7 d, respectivamente. Además, la atenuación del edema vasogénico se acompañó de una mayor preservación de la integridad de la barrera hematoencefálica a 7 días post-reperfusión. En conclusión, nuestros hallazgos describen que el bloqueo del ADRB1 mejora el daño cerebral, identificando así un nuevo objetivo terapéutico para mejorar los resultados en pacientes con accidente cerebrovascular. Esta estrategia terapéutica se encuentra en las primeras etapas de su estudio traslacional y debe explorarse más a fondo en un futuro.

GENERAL INTRODUCTION

Ischemic stroke

Stroke is the second largest cause of mortality worldwide, only surpassed by ischemic heart disease (1). Ischemic stroke is primarily a consequence of carotid and cerebrovascular disease, the latter of which includes both large vessel and small-vessel disease. In addition to larger ischemic strokes produced by thrombosis in carotid or cerebral arteries ($\approx 85\%$), hemorrhagic stroke can also occur ($\approx 15\%$). Microvascular changes during small-vessel disease result in small regions of ischaemia (lacunar infarcts) and microbleeds (2).

The most common stroke symptoms that people present with are facial numbness and weakness, visual impairment, weakness of the upper and lower limbs on one side of the body, impaired balance, nausea, abrupt severe headache and speech impairment. Symptoms mainly depend on the cerebral territory irrigated by the occluded artery (3).

Occlusions of internal carotid artery, M1 and M2 segments of the middle cerebral artery or vertebro-basilar arteries represent 11-29% of acute ischemic stroke (4, 5). Brain hypoperfusion caused by a large vessel occlusion usually results in irreversible death of brain tissue, due to a lack of blood supply, leading to the core infarction. Even so, the core is surrounded by the penumbra (brain tissue that is hypoperfused), but can be salvaged by prompt restoration of blood flow (1, 3).

Reperfusion therapy, either with intravenous (i.v.) recombinant tissue plasminogen activator (rt-PA), endovascular thrombectomy treatment or both, is the only clinically available intervention (6). Endovascular thrombectomy has been recently shown to be successfully used for recanalization in large vessel occlusions (7-9). The exact time of onset of symptoms is critical for determining eligibility for reperfusion therapy (10).

Fast and accurate diagnosis of stroke is vital for selection of the appropriate acute treatment (3). For this purpose, various field triage stroke scales have been developed. However, reliably distinguishing between intracerebral hemorrhage and ischemic stroke can only be done by neuroimaging (10). The primary purpose of neuroimaging is to rule out the presence of other types of central nervous system lesions and to distinguish between ischemic and hemorrhagic stroke. Computerized tomography (CT) scans are considered sufficiently sensitive for detecting mass lesions, as well as acute hemorrhage. By contrast, CT scans may not be sensitive enough to detect an ischemic stroke, whereas multimodal magnetic resonance imaging (MRI) has better resolution than CT and greater sensitivity for detecting it, and it is therefore considered the gold-standard (11, 12).

Magnetic Resonance Imaging

The primary origin of the MRI signal used to generate almost all clinical images comes from hydrogen nuclei. The proton is constantly spinning and so the positive charge spins around with it. Thus, protons have their own magnetic fields (magnetic moment) and behave like little bar magnets. Magnetic moments are normally randomly orientated; however, when an external magnetic field (B_0) is applied, they align either with (parallel) or against (antiparallel) it, with the parallel state being the preferred one. When exposed to B_0 , protons exhibit two relevant phenomena:

- Precession. The overall effect of B_0 on a group of protons means that spins move in a particular way called precession. The speed of precession is measured as the precession frequency and determined by the Larmor equation:

$$\omega_0 = \gamma B_0$$

with γ being a constant for a particular nuclei species (gyromagnetic ratio).

- Longitudinal magnetization. Protons precessing parallel to B_0 result in a sum magnetic field, which is characteristically shown as a vector in the direction of the z-axis, along B_0 .

With the patient being in the magnet and possessing longitudinal magnetization, radiofrequency (RF) pulses are switched on and off, in order to disturb the protons so that they fall out of alignment with B_0 . When the RF pulse has the same frequency as the precessional frequency of the protons, there is transference of energy to the protons (term known as resonance) that induces two main effects on them. Some protons gain energy and move to the higher energy state (antiparallel), thus resulting in a reduction in overall longitudinal magnetization. In addition, the RF pulse causes the protons to move in phase (in same direction at same time) with each other. The result of these effects is the appearance of transverse magnetization, in which a new magnetization vector is created in the x-y plane which precesses at the Larmor frequency (13).

As soon as the RF pulse is switched off, the protons start to fall out of phase with each other and also return to a lower energy state. Relaxation occurs in two different ways: transverse magnetization begins to disappear and the longitudinal one starts to return to its original value (T2 and T1 relaxation, respectively). These two phenomena are simultaneous and independent. The rate at which T1 relaxation occurs is dependent on the tumbling rate of the molecule in which the proton resides. Free water has a small molecular size and tumbles much too quickly to be effective at T1 relaxation. By contrast, fat has a short T1 value because the carbon bonds at the ends of the fatty acids have frequencies near the Larmor frequency, allowing effective energy transfer. Regarding T2 relaxation, there are two causes for the loss of phase coherence: slowly fluctuating magnetic field variations within the local tissue and the inhomogeneity within B_0 . Magnetic field variations result in slightly different Larmor frequencies for protons at different locations within the field. Unlike the random and irreversible process of T2 relaxation, this de-phasing is caused by a constant and is potentially reversible. T2* relaxation is the name given to describe the effects that result from the combination of T2 relaxation and the de-phasing that results from inhomogeneity in B_0 , and determines the actual rate of decay observed when measuring a free induction decay (FID) signal (**Figure 1**) (13).

The signal generated by FID is not usually measured in MRI. Instead, it is common practice to generate and measure the MR signal in the form of an echo: typically a spin echo (SE) or a gradient echo (GRE). Echoes can be appreciated by considering how T1- (T1W) and T2-weighted (T2W) images are formed. T1W images are generated predominantly by manipulating the time between two RF excitation pulses, the so-called repetition time (TR). Application of a 180° RF pulse following an initial 90° RF pulse rotates the protons through 180° , effectively making the protons turn around and precess, still in the x-y plane but in the opposite direction. Eventually, the protons come back into phase, which results in an increase in the amplitude of the MR signal. Maximum signal amplitude is reached at the echo time (TE). As the protons bounce back following the

application of the 180° RF refocusing pulse, the signal obtained is given the name SE. It is possible to repeat the 180° RF refocusing pulse and obtain further SEs (**Figure 1**) (13).

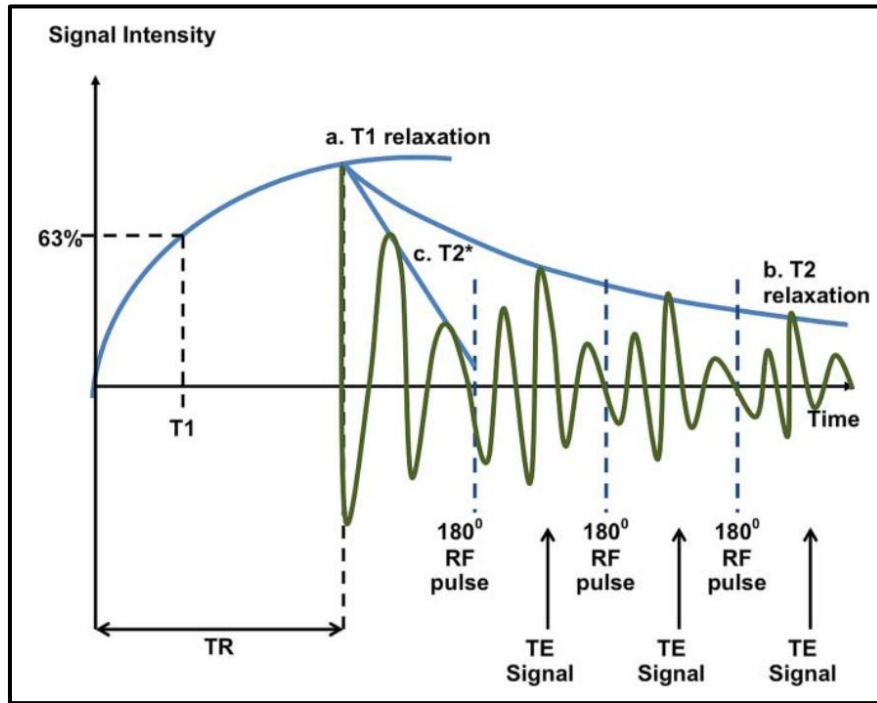


Figure 1. T1, T2 and T2* relaxation. (A) Recovery of longitudinal magnetization over time following the switching off of a RF pulse. (B) T2 curve: An 180° refocusing pulse results in a temporary gain in signal intensity at TE termed SE. Multiple 180° pulses result in a chain of SE. Each subsequent echo will be of lower intensity due to T2 effects. (C) T2* results when 180° refocusing pulses are not used. TR, repetition time, TE, echo time. Figure from Currie S, et al. (2013).

In GRE sequences, magnetic field gradients produce a change in field strength and thus a change in Larmor frequency along a particular direction. Application of a gradient pulse after an initial RF pulse causes protons to rapidly de-phase along the direction of the gradient resulting in rapid decline in the FID signal, which can be reversed by applying a second magnetic field gradient with a slope of equal amplitude but in opposite direction. As a result, protons move back into phase and return a signal called GRE (**Figure 2**). GRE sequences then replace the 180° refocusing RF pulse and are relatively short in comparison with SE with long TR and TE (13).

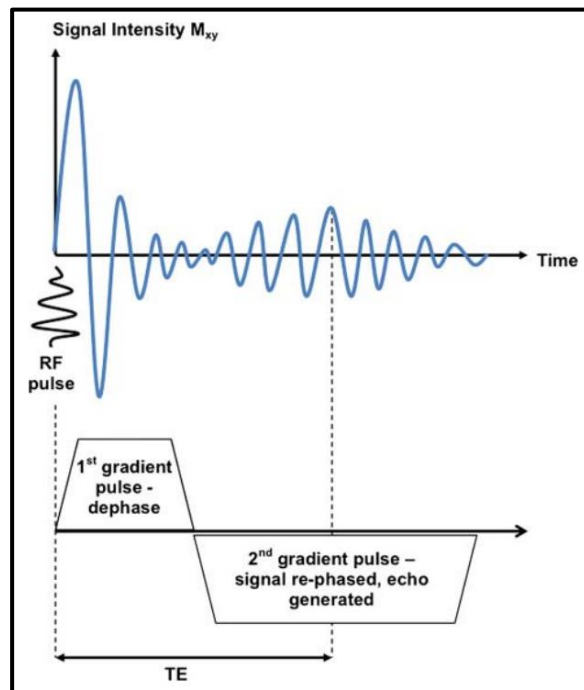


Figure 2. Gradient echo. A RF pulse causes transverse magnetization and initiation of a FID signal. This signal rapidly de-phases following the application of a magnetic field gradient. Application of a second magnetic field gradient with a slope of equal amplitude but in opposite direction to the first causes some rephasing. The signal increases again at time TE to a maximal signal termed a gradient echo. The maximum amplitude of the gradient echo is dependent on the specified TE and the T2*relaxation rate of the tissues in question. TE, echo time. Figure from Currie S, et al. (2013).

Imaging parameters influencing the MR signal in the SE sequence include TE and TR. Short TR and short TE generates a T1W image; short TR allows differences in longitudinal magnetization to develop before the next 90° excitation pulse while short TE limits the T2 effects. Long TR and long TE produces a predominantly T2W image; long TR allows recovery of longitudinal magnetization (thus limiting T1 effects) while at long TE T2 effects become pronounced. A different type of image is produced at long TR and short TE. Long TR and short TE limit T1 and T2 effects, respectively. When this occurs, the signal is predominantly influenced by the proton density of the tissue (13).

Imaging in ischemic stroke

CT is the most widely used diagnostic tool because of its availability and rapid acquisition time (14). A non-contrast CT examination can quickly exclude the presence of hemorrhage. The absence of hemorrhage supports the diagnosis of an ischemic event, and some evidence of ischemia may be seen in the native CT as well (15). During CT perfusion a rapid intravenous infusion of contrast is administered and sections of the brain are repeatedly imaged. Based on the total amount and speed that blood flows to different vascular territories of the brain, this technique can assist in identifying a stroke and potential areas of reversible and salvageable brain tissue in the ischemic penumbra (16).

MRI has advantages over CT as it is usually more sensitive and specific in distinguishing both the stroke mimics and secondary ischemic lesions (15). Diffusion-weighted imaging (DWI) best detects acute ischemia, stroke-like events and is the reference for infarct core extent measurement, which is crucial in selecting patients for endovascular treatment in the later time window. In patients with unknown onset time, MRI identifies strokes that occurred approximately within the previous 4.5 hours and could benefit from thrombolysis (14). Standard T1 and T2 are good at detecting vasogenic oedema that is present in the subacute phase of stroke and is seen at greater than 24 hours to several days. Fast spin echo T2- weighted sequences can clearly demonstrate areas of oedema not visible on the CT and can help identify a subacute stroke (16). MRI drawbacks theoretically include screening time for contraindications, limited access, additional time needed to clear the MRI scan and place the patient on the table, and longer scan duration (14).

Beta-adrenergic receptors and beta-blockers

ADRBs are non-sensory G protein-coupled receptors (class A), which signal through heterotrimeric G-proteins once in contact with adrenergic neurohormones norepinephrine and epinephrine (catecholamines) (17, 18), and play a critical role in the regulation of the function and processes of the cardiovascular system (19). Presently, three different ADRBs subtypes have been described: beta-1 (ADRB1), beta-2 (ADRB2) and beta-3 (ADRB3)-adrenergic-receptors (19), which differ in structure, function, affinity states and pharmacological properties (18, 20-25). ADRB1s are predominantly located in the heart (approximately a 4:1 ratio of ADRB1 to ADRB2), while ADRB2s and ADRB3 are frequently less prominent in cardiomyocytes but are abundant in non-myocyte cells (19), with ADRB2 being found in vascular and bronchial smooth muscle (26) and ADRB3s in the adipocytes where they are involved in fatty acid metabolism (27, 28).

The beta-blocker class of drugs consists of a heterogeneous group of agents with marked variations in their pharmacodynamics and pharmacokinetics, which may translate into potential differences in tolerability, and in hemodynamic and other vascular and metabolic properties. Also known as beta-adrenergic antagonists, beta-blockers lower blood pressure by slowing heart rate with a decrease in cardiac output (29). Although their full mechanism of action is not completely understood, beta-blockers are regulators of cardiovascular homeostasis and, therefore, comprise an essential class of drugs designed to reduce morbidity and mortality in patients with cardiovascular disease (29-31). These pharmacological agents are widely recommended as important parts of antihypertensive regimens as well as preferred therapies for patients at high risk for coronary heart disease, including those with angina, ischemic cardiomyopathy, or congestive HF, and some arrhythmias (29).

Beta-blockers cause competitive blockage of ADRBs avoiding the effects of catecholamines. They are differentiated regarding the greater affinity the drug has for ADRB1 over ADRB2 at usual therapeutic levels (pharmacological selectivity), intrinsic sympathomimetic activity, α -adrenergic receptors-blockade capacity, ability to induce vasodilation, liposolubility and pharmacokinetic profile (31, 32). There have been several beta-blockers developed which may be divided into three distinct generations according to differences in the pharmacological properties.

Cardioprotective effect of metoprolol on AMI

Metoprolol is an (aryloxy)propranolamine-based chemical structure beta-1-selective blocker with no intrinsic sympathomimetic or membrane stabilizer activity, moderate hydrophilic:lipophilic balance and hepatic-dependent metabolism by cytochrome P450 (CYP2D6). The half-life of metoprolol is about 3 to 4 hours in most patients. Orally, there is significant hepatic first-pass elimination, which results in around 50% of the oral dose reaching the systemic circulation, and its moderate lipophilia and reduced polar superficial area allows it to pass through the Blood Brain Barrier (BBB). Historically, metoprolol has been a long-used beta-blocker in the treatment of hypertension, chronic heart failure and acute myocardial infarction (AMI) (32).

In experimental models of AMI, it was shown that i.v. metoprolol exhibited a significant reduction in infarct size (IS) only when administrated before reperfusion (33, 34). Based on these promising results, the METOCARD-CNIC trial was conducted to confirm whether i.v. metoprolol prior

reperfusion was cardioprotective in 270 ST-elevation myocardial infarction (STEMI) patients undergoing percutaneous coronary intervention within the 6 hours of symptoms onset. Patients randomly allocated to receive i.v. metoprolol treatment presented a significant IS reduction measured by cardiac magnetic resonance (CMR) at 5-7 days and improved long-term cardiac function by a follow-up CMR at 6 months (35, 36).

Additionally, post hoc analyses of the METOCARD-CNIC trial revealed that i.v. metoprolol before reperfusion was able to ameliorate electrocardiographic markers of myocardial ischaemia (37), and that the sooner its administration the smaller the IS and the higher the left ventricular ejection fraction (38). Animal studies confirmed these results (38) and proposed i.v. metoprolol as an intervention ideally suited to the treatment of STEMI patients (39).

Neutrophils, Ischemia/Reperfusion Injury and metoprolol

The main determinant of poor outcome after an AMI or ischemic stroke is the extent of irreversible injury (IS). The mainstay of acute myocardial and brain infarction is rapid reperfusion of the occluded artery to restore blood flow mainly by PCI in the case of AMI (40), or pharmacological and/or endovascular therapy in the case of ischemic stroke (6, 41). However, despite being essential for tissue salvage, evidence shows that reperfusion itself triggers a set of potentially deleterious events that contribute to final IS, which is known as reperfusion injury. Overall, the damage inflicted to the tissue is the result of both ischaemia- and reperfusion-related phenomena, and it is known ischaemia-reperfusion injury (IRI) (42-46). Indeed, the development of effective coadjuvant therapies to reduce it is therefore an unmet clinical need (47).

Paradoxically, blood flow restoration in large arteries is not accompanied in many times by efficient tissue perfusion due to the obstruction of the microvasculature. Endothelial swelling, external compression of small vessels secondary to oedema formation, and cellular aggregates (neutrophils, platelets and erythrocytes) generating plugs that restrict tissue perfusion at the capillary level contribute to the phenomenon known as microvascular obstruction (MVO) (48-50). Besides, tissue reperfusion has been shown to accelerate and exacerbate a massive leukocyte infiltration, which is mainly driven by neutrophils that infiltrate the damage tissue through interactions with other cells (e.g. platelets) and contribute to final IS (45, 51-55). Altogether, these phenomena are the major contributors to IRI and final IS.

The mechanism underlying the cardioprotective effect of i.v. metoprolol was deeply unveiled by our group five years ago (56). First, the evaluation of MVO in the cohort of patients of the METOCARD-CNIC trial revealed a significant less incidence and extent in patients receiving i.v. metoprolol before reperfusion. Moreover, the positive association between neutrophil counts and the incidence/extent of MVO in AMI patients was also blunted. Further studies in animal models showed that i.v. metoprolol exerted its infarct-limiting properties through neutrophil stunning and, therefore reperfusion-associated injury: neutrophil infiltration into myocardium was prevented, and no additional cardioprotective effects with i.v. metoprolol were found in neutrophil-depleted mice or when neutrophils were incapable of interacting with platelets. In line with these findings, i.v. metoprolol abrogated neutrophil infiltration and disrupted intravascular cell behavior in mice

models of sterile inflammation, thus abrogating deleterious neutrophil-driven responses (**Figure 3**) (56).

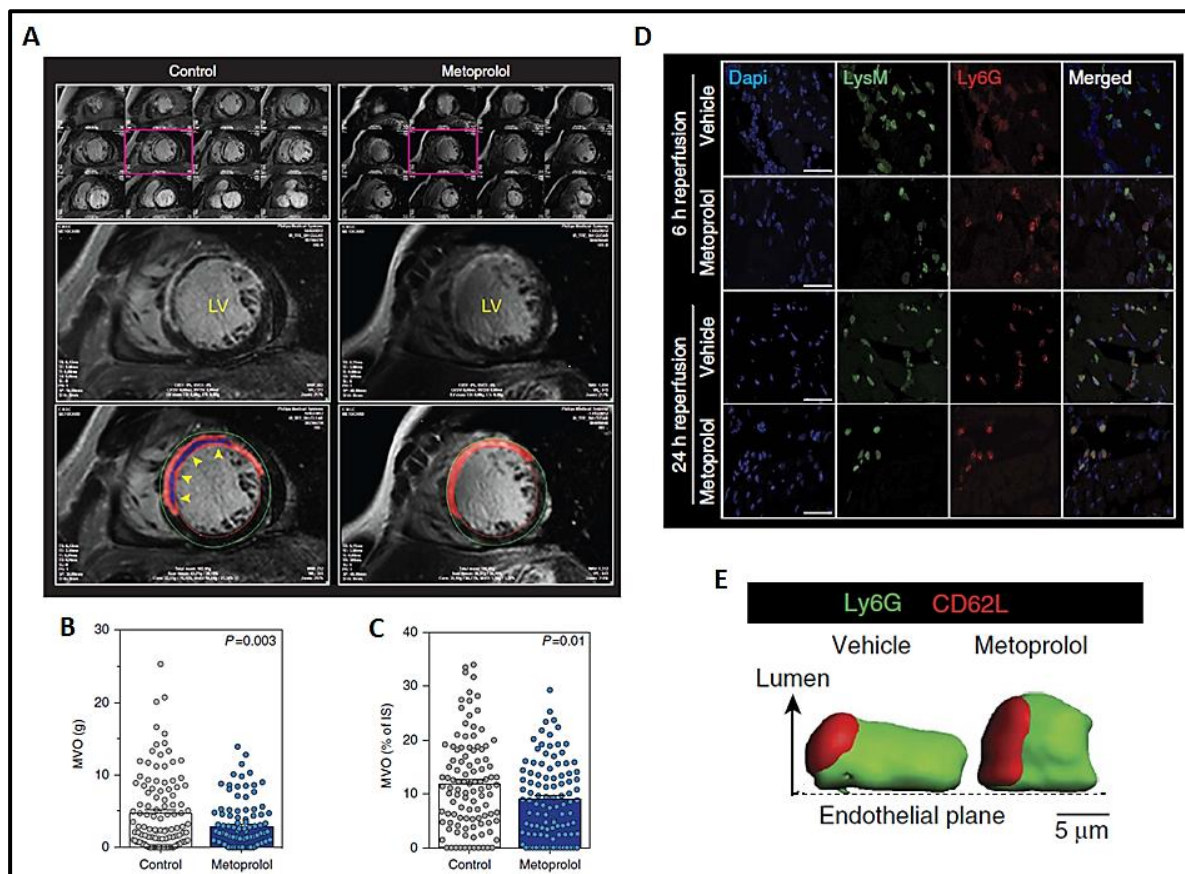


Figure 3. Neutrophil stunning by metoprolol is cardioprotective. (A) Representative CMR images, showing differences in 1-week MVO between a control patient (left) and a metoprolol-treated patient (right). Quantification of MVO in grams of LV (B) and relative to the infarcted area (%) (C). (D) Representative confocal images of LV sections taken from injured mice after 6 and 24 hours reperfusion onset. Myeloid infiltration (LysM-GFP⁺, green), most of which are neutrophils (Ly6G⁺, red), was attenuated in metoprolol-treated mice. (E) 3D reconstructions of neutrophils within live vessels of vehicle- and metoprolol-treated mice (red, uropod; green, neutrophil cell body), which represent reduced elongation (prolate ellipticity) and enhanced projection of recruited neutrophils into the luminal space (height-to-length ratio). Figure adapted from García-Prieto J., et al. (2017).

OBJECTIVES

Pre-reperfusion administration of i.v. ADRB1-blocker metoprolol is a safe strategy that reduces myocardial IS through neutrophil stunning and improves long-term cardiac function. Based on this previous evidence generated in our laboratory, and on the relevance of neutrophils in cerebral I/R injury in which exacerbated neutrophil-mediated inflammation has been linked to increase IS, blood-brain barrier (BBB) disruption, hemorrhagic transformation (HT) and worse neurological outcomes, the main hypothesis tested on this work is that i.v. metoprolol exerts a beneficial effect in the context of reperfused ischemic stroke.

The objectives set to test this working hypothesis are:

1. To perform a longitudinal analysis by MRI to study the beneficial effect of the selective ADRB1 blockade against ischemic stroke (e.g. cerebral I/R injury) in terms of IS reduction, oedema attenuation, and BBB integrity preservation.
2. To confirm whether the protective effect of metoprolol administration evaluated by MRI is consistent with histopathological analyses using optical imaging (immunohistochemistry and immunofluorescence).

MATERIAL AND METHODS

Animals

All experimental and other scientific procedures with animals conformed to EU Directive 2010/63EU and Recommendation 2007/526/EC, enforced in Spanish law under Real Decreto 53/2013. Animal protocols were approved by the local ethics committees and the Animal Protection Area of the Comunidad Autónoma de Madrid.

Rat procedures

Rats were maintained under pathogen-free conditions in a temperature-controlled room and a 12-hour light-dark cycle in the animal facility of Hospital General Universitario Gregorio Marañón, Madrid, Spain (ES280790000087). Chow diet and water were available ad libitum. We subjected 76 8-10-week-old wild-type male Wistar rats to middle cerebral artery occlusion and reperfusion (MCAO/R) injury. Rats weighed around 200-250 g by the moment the stroke was induced. Animals were randomized by simple randomization to receive a pre-reperfusion 12.5 mg/kg i.v. bolus of metoprolol-tartrate (M5391, Sigma) or vehicle (saline, 0.9% NaCl). A subgroup of 55 rats was monitored by MRI during middle cerebral artery occlusion/reperfusion (MCAO/R) (baseline) and at 24 h and 7 d post-reperfusion, followed by sacrifice and removal of the brain for immunohistochemical analysis. The remaining 21 rats were monitored under the same MRI protocol, but were sacrificed after the 24 h post-reperfusion scan for analysis of neuroinflammation by immunohistochemistry. The selected i.v. metoprolol dose was based on a dose-response study in rats showing a moderate hemodynamic effect (< 20%) (56). In the MCAO/R model, mortality reached 30% within 24 h post-reperfusion (16% and 14% for vehicle and metoprolol, respectively).

The study protocol stipulated the exclusion of rats with a quasi-hemispheric infarct (IS > 40%) at 24 h. This occurred in 9% of the rats (4% and 5% in the vehicle and metoprolol groups, respectively). MRI in these rats showed a midline shift or hemorrhage at 7 d post-reperfusion. Another animal was excluded due to a large cerebral hemorrhage at 24 h post-reperfusion. In addition, 13% of rats were excluded due to failure of the surgical model, as determined by absence of infarct on T2W MRI images at 24 h post-reperfusion. Therefore, 46% (16 and 19 in the vehicle and metoprolol groups, respectively) of rats subjected to MCAO/R had IS <40% and were included in the evaluation of the neuroprotective effect of the early i.v. metoprolol.

An additional group of rats was performed for neurological assessment up to 21d after stroke. In this batch of rats, BBB permeability was evaluated by two different MRI methods at 24 h and 7 d post-reperfusion.

Cerebral ischemia-reperfusion injury

The intraluminal MCAO/R model is the gold-standard for surgical modeling of ischemic stroke. In our protocol, rats were anesthetized with 3% sevoflurane in 100% O₂ via a facemask throughout surgery and intraluminal occlusion. Immediately before surgery, animals received a single dose of 0.3 mg/kg of i.p. fentanyl. The carotid artery was then exposed, and an intraluminal 4-0 suture (Doccol, 404134PK10) was advanced via the internal carotid artery to occlude the base of the

middle cerebral artery (MCA). Rats were subjected to 35 min ischemia and randomized to receive a single i.v. bolus of vehicle or metoprolol (12.5 mg/kg) 10 min before reperfusion. After the 35 min ischemia, the suture was retracted to reinstate blood flow in MCA-supplied brain territories. After incision closure, rats received 2 ml of warm saline (0.9% NaCl) subcutaneously (s.c.) as volume replacement. After the procedure, rats were placed in a warm recovery cage to prevent hypothermia, with free, easy access to food and water. To prevent pain, 0.1 mg/kg of buprenorphine was administered s.c. immediately after surgery and 24 h and 48 h post-surgery. Rats were kept under observation and monitored by MRI at different times post-reperfusion, as explained below.

Brain magnetic resonance imaging

Brain MRI scans were obtained with a 7 Tesla BioSpec 70/20 scanner (Bruker, Germany). Images were acquired using a volume coil for signal transmission and a 4-element rat-head surface coil for signal reception. Animals were maintained throughout the procedure under sevoflurane anesthesia (5% induction and 3% maintenance, in 100% O₂). Axial and coronal T₂-weighted images and diffusion-weighted images (DWI) were acquired at 24 h and 7 d post-reperfusion. Besides, to evaluate the BBB permeability, coronal T₁-weighted sequences were acquired at 24 h and 7 d post-reperfusion before and after the injection of the contrast agent. Additionally, dynamic contrast enhancement images were acquired and fit to a pharmacokinetic modeling to estimate K_{trans} and K_{ep} parameters (57). To assess the hypoperfusion area, a dynamic susceptibility contrast (DSC) perfusion-weighted sequence was also acquired during MCAO.

Parameters of each sequence were as follows. For T₂W MRI images, a RARE sequence was acquired with TR = 6741.2 ms, TE = 30 ms, 4 averages, rare factor = 8, slice thickness = 0.4 mm, FOV = 35 x 35 mm², and matrix size = 256 x 256 pixels. DWI study was based on a single shot echo-planar imaging with TR = 3000ms, TE = 21 ms, 1 average, b values = 0 and 650 s/mm², slice thickness = 1 mm, FOV = 30 x 25 mm², and matrix size = 128 x 64 pixels. Additionally, during the infarct, DSC perfusion-weighted images were dynamically acquired during an i.v. injection of 0.5mmol/kg Gd contrast agent (ProHance, Bracco Diagnostics) in 0.2 ml administered at 2.4ml/min with TR = 700 ms, TE = 7.715 ms, 1 average, 100 repetitions, slice thickness = 1 mm, FOV = 30 x 25 mm², and matrix size = 92 x 50 pixels. In a subgroup of animals at 24h and 7d in addition to T₂ and DWI images, pre- and post-contrast T₁W MRI images, a 3D-FLASH sequence was acquired with TR = 40 ms, TE = 8, flip angle 30°, 1 average, FOV = 34x34x24 mm³, and a matrix size = 114x114x20 pixels, before and after the contrast injection, respectively. During contrast injection (0.5 mmol/Kg Gd in 0.15ml at 1ml/min), dynamic T₁W images were acquired with a temporal resolution of less than 5 seconds each dynamic (TR: 4.076 ms, TE = 1.822 ms, FOV = 25x21x24 mm³ and a matrix size = 76x64x20 pixels). To properly assess the contrast wash-out, 40 volumes were acquired for 3':18''.

Infarct size and oedema quantification

Infarct volume at 24 h and 7 d post-reperfusion was quantified from coronal T2W MRI images. Infarct regions were selected as hyperintense areas. Area at risk (AAR) was calculated by analyzing DSC perfusion-weighted MRI images obtained during MCA occlusion, before reperfusion. Ipsilateral hypoperfused areas were detected as notably hypointense regions compared with the perfused contralateral hemisphere.

Parametric apparent diffusion coefficient (ADC) maps were obtained from DWI MRI images captured at baseline and 24 h and 7 d post-reperfusion. Cytotoxic oedema (intracellular) was identified as hypointense regions, mainly observed after MCAO and at 24 h post-reperfusion. Regions of interest (ROI) were transformed into volumes by taking account of the slice thickness. Vasogenic oedema (extracellular) was identified as hyperintense regions at 7 d post-reperfusion. Since vasogenic oedema was mainly restricted to basal ganglia, we quantified its presence by comparing the ipsilateral (infarct) and contralateral intensities of this region in one slice per rat in ADC maps and T2W images (-0.36/-0.96 mm Bregma interval).

Because vasogenic oedema is related to a decrease in BBB integrity, we quantified the permeability of the BBB by comparing the ipsilateral (infarct) and contralateral intensities of this region in one slice per rat in T1W images (-0.36/-0.96 mm Bregma interval). Contrast enhancement ratio was computed normalizing the subtraction between post and pre contrast images over the pre-contrast images per each animal. For DCE images a ROI was placed at the artery (PONER images) to estimate the arterial input function (AIF) and two additional ROIs were placed at the same anatomical regions to extract time intensity curves. Toft and Kermode model assumes that the equilibrium concentration of gadolinium in whole tissue (C_t) is driven by passive diffusion based on its concentration difference between the plasma (C_p) and tissue extracellular space (C_e). Intensity curves were fitted to Toft model (57) following:

$$C_t(t) = K_{\text{trans}} \int_0^t C_p(\tau) e^{-k_{\text{ep}}\tau} d\tau$$

where C_p is the contrast at the artery, C_t is the contrast enhancement at the parenchyma ROIs, K_{trans} is the efflux rate of contrast that enters from blood plasma into brain parenchyma, which is closely related to BBB permeability, and K_{ep} is the contrast washout rate of the contrast from the extravascular-extracellular space back to blood plasma. The non-linear convolution signal modeling was performed using non-linear fitting algorithm available in Excel. From this analysis the extracellular volume (ECV) can be computed as the ratio between the K_{trans} and K_{ep} :

$$\text{ECV} = \frac{K_{\text{trans}}}{k_{\text{ep}}}$$

Final IS was calculated as the ratio of infarct volume to the AAR. In an alternative approach, IS was calculated by considering the at-risk tissue as a perfusion-diffusion mismatch (PDM) (58); in this approach, IS was calculated as the ratio of infarct volume to PDM. Infarct volumes estimated from T2W MRI images were also compared between groups at different time-points without normalization. MRI analyses were carried out by a blinded trained researcher.

Rat carotid artery catheterization and hemodynamic dose-response characterization

Animals were weighed and anesthetized (xylazine 20 mg/Kg i.p.; ketamine 60 mg/Kg i.p.). Systemic arterial blood pressure and heart rate were measured via a catheter (filled with heparinised saline 10U/ml) inserted through the carotid artery. This catheter was connected to a Transpac® IV (ICU Medical) pressure transducer linked to a MP36 data acquisition system and measurements were recorded using Acqknowledge data analysis software (Biopac Systems, Inc.). Crescent cumulative doses of metoprolol (3.13, 6.25, 12.5, 25, 50, 100, 150 and 200 mg/Kg) were intravenously administered via femoral artery. BP and HR were measured at baseline and 5 min after each dose administration. At the conclusion of the experiment, the catheter was removed by gently pulling it back through the stab wound, and the animal was euthanized. Animals were maintained at 36.5°C throughout the experiment.

Tissue processing

At 24 h and 7 d post-reperfusion, rats were anesthetized by intraperitoneal injection of a mixture of ketamine (100mg/kg) and xylazine (5mg/kg). Rats were then transcardially perfused first with saline-heparin and second with 4% paraformaldehyde. Brains were removed and fixed in 4% paraformaldehyde for 24 h and processed for staining.

Rat brain staining and quantification

Fixed brains were cryoprotected in sucrose and frozen at -80°C. Free-floating cryostat sections (30 µm) were cut and stored in cryoprotectant buffer solution at -80°C until use. Brain infarcts extended from Bregma positions 2.04 to -2.92 mm according to the rat brain in stereotaxic coordinates atlas (59). The 3 sections analyzed per rat corresponded approximately to 3 distinct anteroposterior positions within in this brain-infarct Bregma interval. All immunohistochemical analyses therefore covered the territory affected by the MCA occlusion (60, 61).

Diaminobenzidine (DAB) immunohistochemical analysis was performed as previously described (62) using the following primary antibodies: monoclonal rabbit anti-neuronal nuclear antigen (NeuN) (ab177487; Abcam), polyclonal rabbit anti-aquaporin-4 (AQP4) (A5971, Sigma-Aldrich), polyclonal goat anti-ionized calcium binding adaptor molecule 1 (Iba1) (ab5076; Abcam), polyclonal rabbit anti-PMN (LSBio, LS-C348181-2), polyclonal rabbit anti-glial fibrillary acidic protein (GFAP) (Z0334, Agilent Dako, Santa Clara, CA, USA), monoclonal mouse anti-chondroitin sulfate proteoglycan (CSPG) (Cat-315, MAB1581, Sigma-Aldrich, Merck Millipore), and polyclonal rabbit anti-myelin basic protein (MBP) (GTX133108; GeneTex). IgG extravasation analysis was performed using a goat anti-rat IgG biotinylated antibody (BA-9401-.5; Vector Laboratories). For double immunohistochemistry (IHC), sections already stained for GFAP or MBP and developed with DAB were then incubated with the anti-CSPG antibody. The CSPG signal was detected with the ImmPRESS®-alkaline phosphatase horse anti-mouse IgG polymer detection kit (MP-5402, Vector Laboratories) and Vector Blue substrate (SK-5300, Vector Blue Alkaline Phosphatase Substrate Kit). All IHC slides were scanned by the CNIC histopathology service using

the NanoZoomer-2.0-RS digital slide scanner (C110730®, Hamamatsu, Japan) and visualized with NanoZoomer Digital Pathology software (Hamamatsu). Images were exported and quantified using ImageJ (NIH, Bethesda, MD, USA).

To determine neuronal preservation in infarcted brain hemispheres, brains removed at 7 d post-reperfusion were stained for neuronal nuclei with anti-NeuN antibody. ROIs were manually drawn to cover territories with neuronal loss. To study BBB preservation (AQP4 and IgG), CSPG deposition, myelin sheaths integrity and microglia activation, images were thresholded, and the positive area fraction in every section was averaged per rat. Glial scar formation was determined in ROIs lacking astrocyte staining and surrounded by hypertrophic astrocytes. Double-staining for CSPG plus GFAP or MBP was used to reveal filling of glial scars with proteoglycan matrix and deteriorated myelin sheaths; because proteoglycan deposition and myelin sheath degradation are largely restricted to the basal ganglia, these variables were studied in a ROI drawn around these structures. Images were then thresholded, and the mean positive area fraction was calculated from all sections and normalized to the AAR in each rat. Values were then averaged per group. Data are presented as the fold-change relative to the mean value for the vehicle-treated group. The threshold value that best highlighted the positive area was carefully selected for each marker (198 for AQP4, 215 for IgG, 220 for Iba1, 188 for CSPG and 187 for MBP), and threshold values for every marker were maintained for image quantification in all experimental groups.

For quadruple GFAP+AQP4+Iba1+CSPG immunofluorescence (IF), floating sections were blocked in PBS containing 0.25% Triton X-100 and 3% normal donkey serum and then incubated overnight at 4°C with anti-AQP4, anti-Iba1, and anti-CSPG antibodies. For triple immunofluorescence for GFAP+AQP4+Iba1, IgG+AQP4+Iba1, or GFAP+MBP+NeuN, floating sections were blocked in PBS containing 0.25% Triton X-100 and 3% normal donkey serum (for anti-AQP4 and anti-Iba1) or goat serum and then incubated overnight at 4°C with anti-AQP4 plus anti-IgG, anti-Iba1, or anti-MBP plus anti-NeuN. After these primary antibody incubations, sections were then incubated for 1 h with the corresponding Alexa Fluor (AF)-conjugated secondary antibodies, followed by overnight incubation with mouse monoclonal anti-GFAP AF488 antibody (53989280; clone GA5; eBioscience).

All slides for IF were DAPI counterstained to visualize nuclei, mounted on Superfrost Plus slides (Thermo Fisher Scientific), and covered with Fluoroshield (F6182, Sigma). Images were acquired in the CNIC Microscopy Unit with a Leica TCS SP5 or SP8 Confocal and gSTED 3D System (Leica Microsystems, Mannheim, Germany) fitted with an HC PL APO 63x/1.40 Oil CS2 objective. GFAP, AQP4, Iba1 Z-stacks were acquired with this system according to Nyquist criteria and deconvoluted with Huygens Professional Software version 19.04.0p2 64b (Scientific Volume Imaging B.V., Hilversum, The Netherlands) using the Good's Roughness Maximum Likelihood Estimation algorithm. A 3D Surface element was created with Imaris 9.1.2 Software (Bitplane AG, Zurich, Switzerland).

Statistics

Sample size was calculated by power analysis. Data are presented as mean \pm standard error of the mean (SEM) and were analyzed with Prism software 8.0.1 (Graph pad, Inc.). Normality tests (Shapiro-Wilk test) were used to determine if variables followed a normal distribution. Comparisons between two treatments (e.g. vehicle and metoprolol) were made by 2-tailed unpaired Mann-Whitney for non-normally distributed data or Student's t-test for variables with a normal distribution. Comparisons between 24 h and 7 d post-reperfusion were made by paired Student's t-test. Differences were deemed statistically significant at P values below 0.05: * $p < 0.05$, ** $p < 0.01$, *** $p < 0.001$.

RESULTS

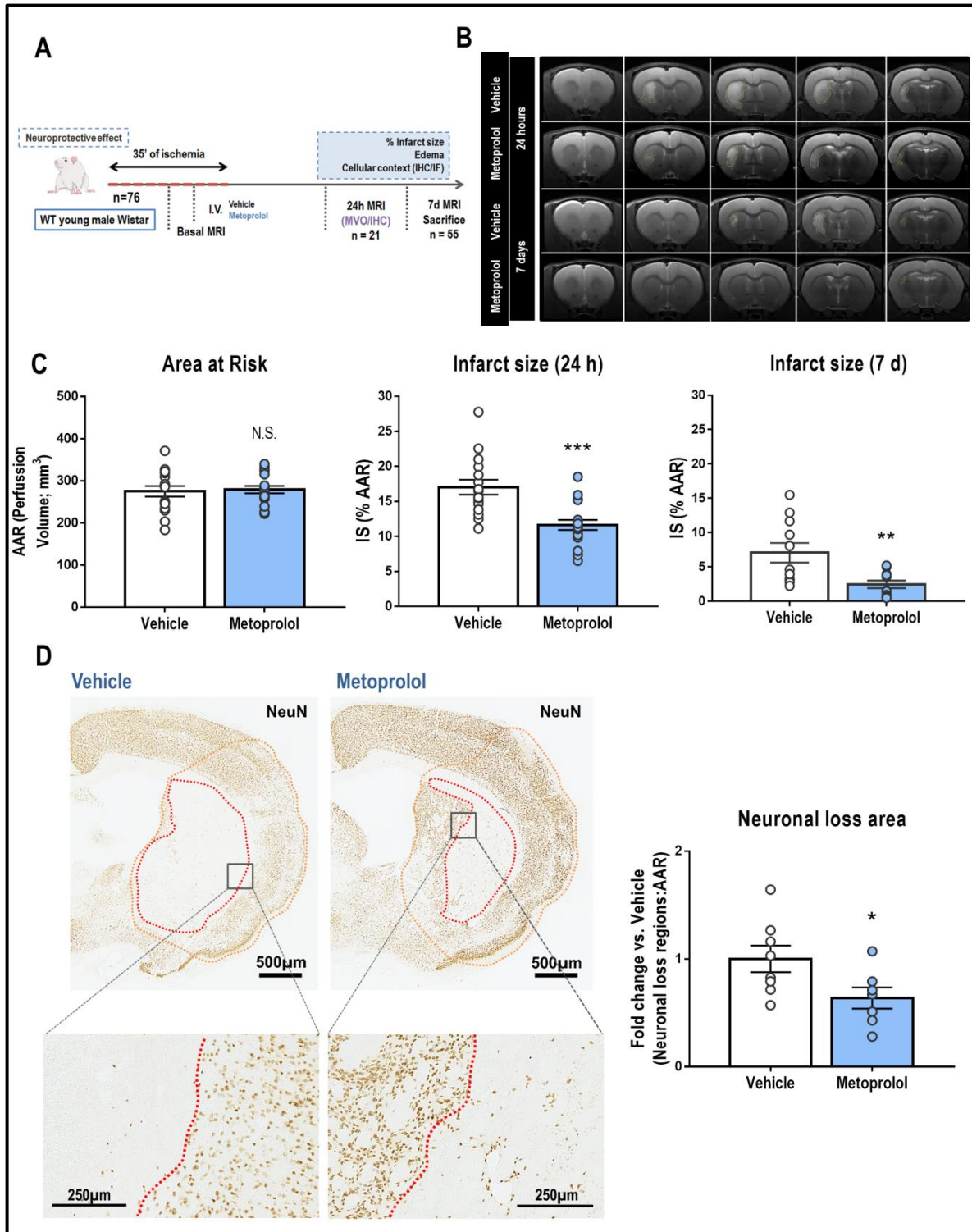
Selective ADRB1 blockade during ongoing stroke reduces brain injury, prevents neuronal loss and improves neurological outcomes

Rats subjected to 35 min of middle cerebral artery occlusion received a single i.v. injection of the selective ADRB1 blocker metoprolol (12.5 mg/kg) (56) or saline (0.9% NaCl, vehicle) 10 min before reperfusion (**Figure 4A**). The selected i.v. metoprolol dose was based on a dose-response study showing a moderate hemodynamic effect on PA and HR (< 20%) (**Figure S1**). Rats underwent 3 MRI studies: during ongoing cerebral ischemia and 24 h and 7 d after reperfusion. The extent of cerebral ischemia provoked by MCAO (area at risk, AAR) was determined from MRI DSC images obtained during occlusion, and did not differ between groups (275.0 ± 12.5 mm³ and 279.1 ± 8.85 mm³ for vehicle- and metoprolol-injected rats, respectively, **Figure 1C**) (**Figure S2**). Brain IS was measured as the AAR-normalized extent of oedema on T2-weighted MRI images at 24 h post-reperfusion (pre-specified primary outcome) and at 7 d post-reperfusion (**Figure 4B**). MRI-quantified IS was significantly smaller metoprolol-treated rats both at 24 h ($17.0 \pm 1.06\%$ of the AAR in vehicle-treated rats vs. $11.6 \pm 0.72\%$ in metoprolol-treated rats, $p < 0.001$, **Figure 4C**) and on day 7 (vehicle, $7.07 \pm 1.42\%$; metoprolol, $2.46 \pm 0.56\%$; $p < 0.01$, **Figure 4C**). Immunohistochemical analysis of the neuronal marker NeuN at 7 d post-reperfusion showed that early i.v. metoprolol administration was associated with significant smaller regions of neuronal loss than observed in the vehicle-treated group (vehicle 1.00 ± 0.11 ; metoprolol, 0.65 ± 0.09 ; $p < 0.05$, **Figure 4D**).

The exclusion of rats with hemispheric infarcts (IS > 40%) was an a priori exclusion criterion defined before experimentation. To rule out unintentional selection bias, we performed a post-hoc analysis of all rats, including those meeting the exclusion criterion, at 24 h post-reperfusion and metoprolol maintained its association with significantly smaller IS (**Figure S3**).

IS was also quantified as a percentage of PDM, another validated normalization method. The results were consistent with IS/AAR data, with metoprolol-treated rats having significantly smaller infarcts at 24 h and 7 d post-reperfusion (**Figure 5A**). Furthermore, comparison of infarct volumes on T2W MRI without normalization also showed that metoprolol-infused rats had significantly smaller infarcts at 24 h and 7 d post-reperfusion (**Figure 5B**).

Figure 4. ADRB1 blockade by metoprolol reduces infarct size and neuronal loss. (A) Rat model of middle cerebral artery occlusion–reperfusion (MCAO/R), with euthanasia at 7 d post-reperfusion. WT, wild-type, MRI, magnetic resonance imaging, IF, immunofluorescence; IHC, immunohistochemistry; MVO, microvascular obstruction. (B) Comparative coronal T2-weighted (T2W) MRI at 24 h (top rows) and 7 d (bottom rows) post-reperfusion. Infarcted regions correspond to hyperintense areas. (C) Infarct size (IS) evaluated by coronal T2W MRI at 24 h (vehicle, n = 16; metoprolol, n = 18) and 7 d post-reperfusion (vehicle, n = 11; metoprolol, n = 11). Final IS was calculated as the ratio of infarct volume to the area-at-risk (AAR) and expressed as %. (D) IHC of coronal sections with anti-NeuN antibody. Higher magnifications of infarcted areas show territories of complete neuronal loss (delineated in red). Neuronal loss analysis in the middle cerebral artery territory (MCA, delineated in orange) of infarcted hemispheres shows neuronal preservation in metoprolol-treated rats at 7 d post-reperfusion (vehicle, n = 8; metoprolol, n = 7). Graphs show mean \pm S.E.M. * $P < 0.05$; unpaired Mann Whitney or Student t-test.



To study whether the neuroprotective effect of metoprolol was consistent with better neurological outcomes, a longitudinal study was performed to evaluate long-term effects of brain injury on sensory-motor behaviors. The results obtained with the motor and behavioral scales (**Figure S4**), firstly showed a slow recovery on these neurological functions over the time in the groups subjected to ischemia (metoprolol and vehicle groups), with no affection in the sham group. With both scales,

despite a better neurological function was observed in the group treated with the drug in all time points, it was not until 21d after the surgery when significant differences were observed, in particular in the behavioral test. Our evaluation of the sensorimotor functions using the adhesive removal test, again revealed an improvement in these neurological deficits in rats receiving i.v. metoprolol, with significant differences at 24h and 7d between these groups in the parameter of time for the first attempt to remove the adhesive.

The results obtained with the cylinder test did reveal a neurological improvement only in the use of the contralateral forepaw at day 7, but no differences were further observed in none of the different time points analyzed, or in any of the others parameters studied.

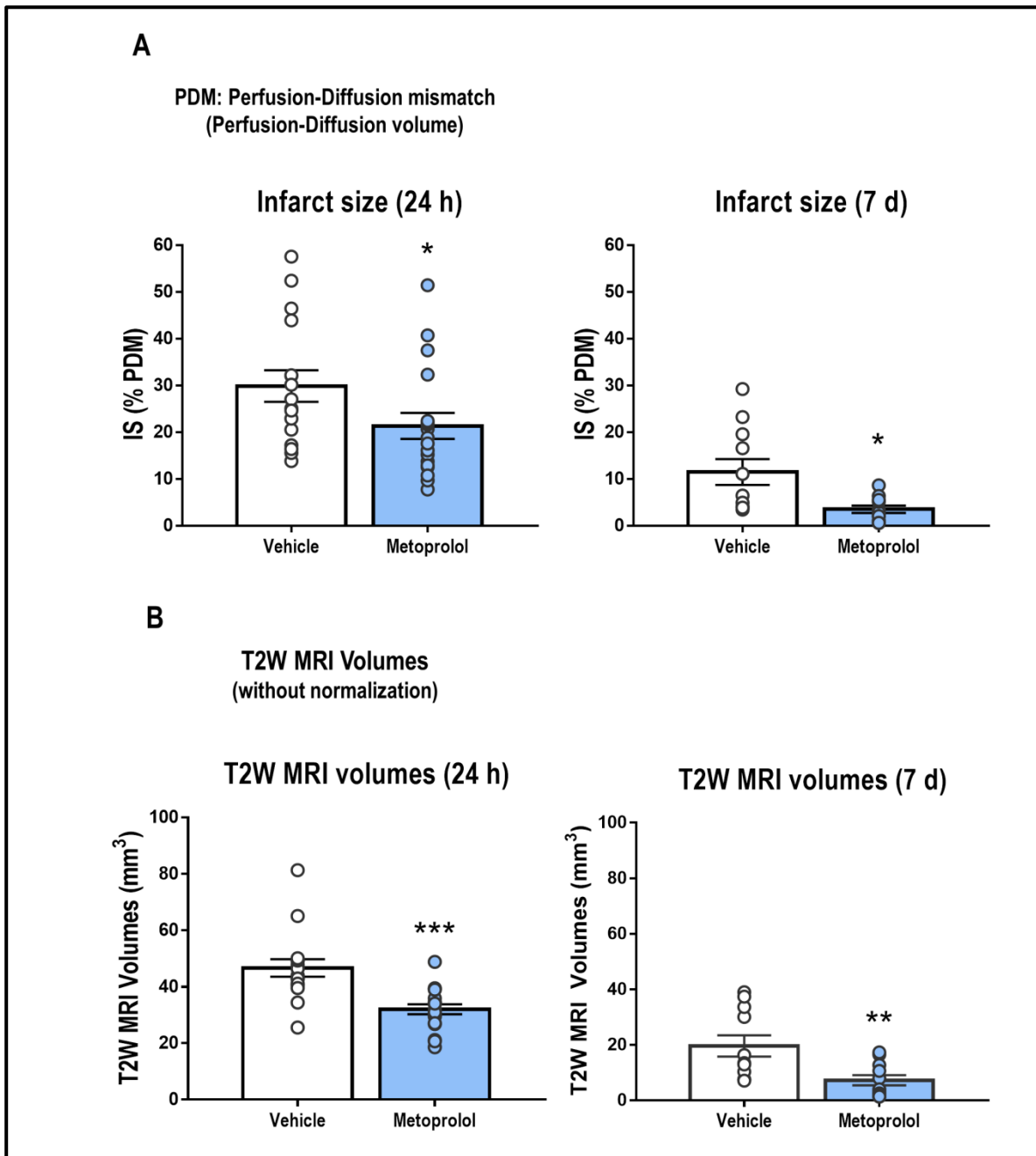
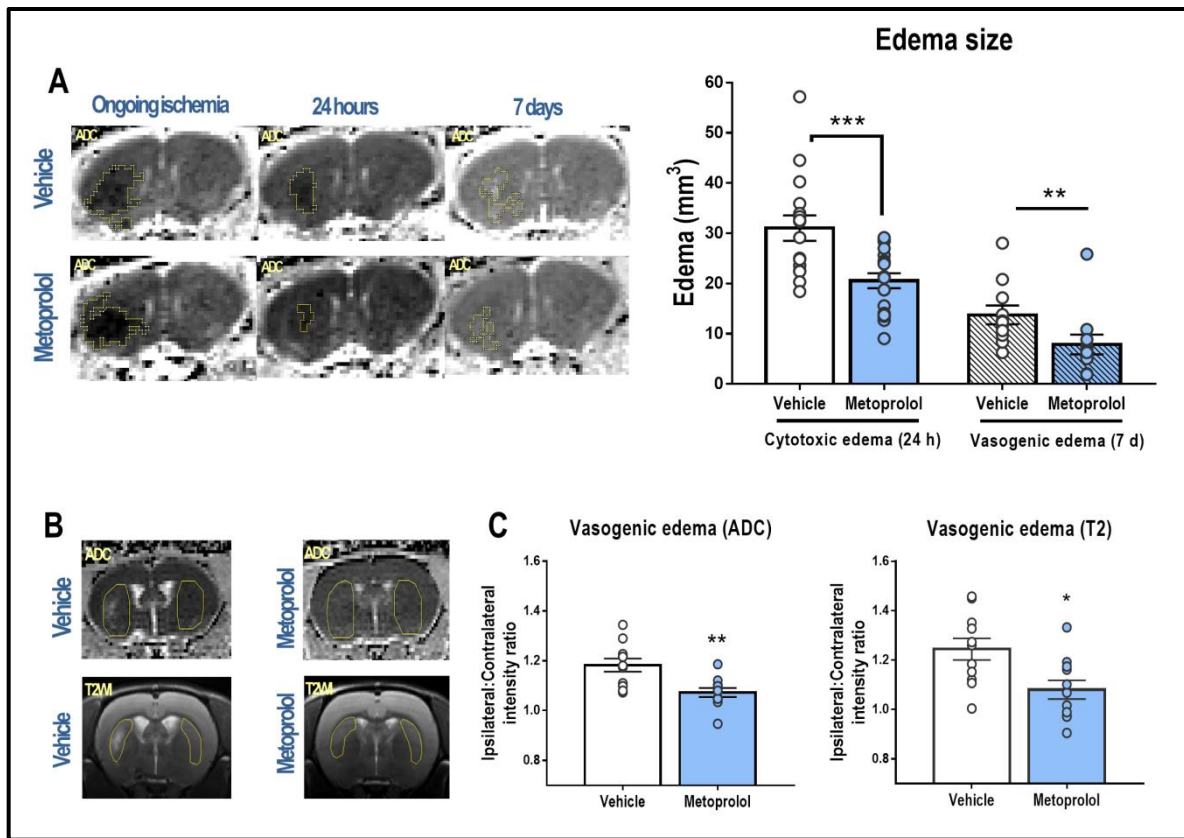


Figure 5. ADRB1 blockade by metoprolol is protective independently of how IS is quantified by MRI. (A) IS normalized to at-risk-to-infarction tissue assessed as perfusion-diffusion mismatch (PDM). The results were similar to those obtained by normalization to area-at-risk (AAR) (see Fig. 1) at 24 h post-reperfusion (vehicle, $29.9 \pm 3.39\%$; metoprolol, $21.4 \pm 2.79\%$; $p < 0.05$) and 7 d post-reperfusion (vehicle, $11.5 \pm 2.78\%$; metoprolol, $3.55 \pm 0.78\%$; $p < 0.05$). (B) Non-normalized T2-weighted MRI infarct volumes; the benefit of metoprolol is still evident at 24 h post-reperfusion (vehicle, 46.7 ± 3.11 mm³; metoprolol, 32.0 ± 1.77 mm³; $p < 0.005$) and 7 d post-reperfusion (vehicle, 19.6 ± 3.84 mm³; metoprolol, 7.29 ± 1.83 mm³; $p < 0.05$), indicating that IS was not conditioned by either AAR or PDM. Data are means \pm S.E.M. * $p < 0.05$, ** $p < 0.01$, *** $p < 0.005$; unpaired MannWhitney or Student t-test.

ADRB1 blockade reduces brain cytotoxic and vasogenic oedema

The extent of cytotoxic and vasogenic oedema was detected as areas of reduced or increased diffusion, respectively, on MRI apparent diffusion coefficient (ADC) maps (16). MRI during index ischemia (before metoprolol or vehicle injection) showed no differences in brain cytotoxic oedema (vehicle, 98.1 ± 8.8 mm³; metoprolol, 105.2 ± 11.7 mm³). At 24 h after reperfusion, metoprolol-treated rats had significantly less cytotoxic oedema than their vehicle-treated counterparts (vehicle, 31.0 ± 2.54 mm³; metoprolol, 20.6 ± 1.62 mm³; $p < 0.01$). Besides, metoprolol-treated rats had a significantly smaller extent of vasogenic oedema at 7 d post-reperfusion (vehicle, 13.8 ± 1.87 mm³; metoprolol, 7.86 ± 1.97 mm³; $p < 0.01$) (**Figure 6A**). Vasogenic oedema was further assessed by comparing ipsilateral and contralateral tissue water content at 7 d post-reperfusion (**Figure 6B**). MRI ADC maps revealed lower water content (ipsilateral:contralateral intensity ratio) in the brain tissue of metoprolol-injected rats (vehicle, 1.18 ± 0.03 ; metoprolol, 1.07 ± 0.02 ; $p < 0.01$; **Figure 6C**). Similar results were obtained by T2W MRI analysis (vehicle, 1.24 ± 0.04 ; metoprolol, 1.08 ± 0.04 ; $p < 0.05$; **Figure 6C**).

Figure 6. ADRB1 blockade by metoprolol reduces brain cytotoxic and vasogenic oedema. (A) Coronal parametric MRI apparent diffusion coefficient (ADC) maps comparing rats receiving i.v. vehicle (top row) or metoprolol (bottom row) during ongoing ischaemia and 24 h and 7 d post-reperfusion. Restricted diffusion was identified at 24 h as hypointense areas and increased diffusion at 7 d as hyperintense areas (outlined in yellow). Metoprolol reduces cytotoxic oedema at 24 h post-reperfusion (vehicle, $n = 16$; metoprolol, $n = 18$) and vasogenic oedema at 7 d post-reperfusion (vehicle, $n = 11$; metoprolol, $n = 11$). (B) Tissue water content analyzed by comparison of ipsilateral (with infarct) and contralateral (without infarct) intensities in similar-sized areas (yellow outlines), in a single slice per rat on ADC maps and T2W MRI. (C) Quantification of ipsilateral-to-contralateral intensity ratios from ADC maps and T2W images, showing reduced brain water content in metoprolol-treated rats. Graphs show mean \pm S.E.M. * $P < 0.05$; unpaired Mann Whitney or Student t-test. Other abbreviations as in Figure 1.



ADRB1 blockade preserves BBB integrity

BBB integrity was evaluated using permeability imaging (DCE), which involved the repeated acquisition of T1W MRI following an i.v. injection of a contrast agent (gadolinium). The analysis of pre- and post-contrast images revealed an increase in BBB permeability at 7 d when compared to 24 h post-reperfusion (24 h, 1.18 ± 0.38 ; 7 d, 4.58 ± 2.62 ; $p=0.06$; **Figure 7A, 7C**). Consistently, DCE images analysis showed a trend towards the increase in ECV (**Figure 7C**). When the integrity was assessed in metoprolol-treated rats, our results showed a significant BBB preservation at 7 d post-reperfusion. Similar results were obtained between both analyses of pre- and post-contrast T1W (vehicle, 4.58 ± 2.62 ; metoprolol, 1.41 ± 0.17 ; $p<0.05$; **Figure 7B, 7D**) and DCE images (vehicle, 0.26 ± 0.02 ; metoprolol, 0.21 ± 0.01 ; $p=0.06$; **Figure 7D**). This ECV increase in the vehicle group was mediated by a worse BBB as it is reflected by a trend in the K_{trans} and slower contrast washout (lower K_{ep}) (**Figure 7D, Figure S5**).

Additionally, we assessed BBB integrity by immunohistochemical analysis of AQP4, whose expression on the end-feet of astrocytes in the BBB prevents post-stroke neuroinflammation-related oedema (63). AQP4 expression at day 7 post-reperfusion was 2-fold higher in metoprolol-treated rats (vehicle, 1.00 ± 0.24 ; metoprolol, 2.00 ± 0.41 ; $p<0.05$; **Figure 7E, 7G**). These results were consistent with an increase of IgG extravasation in the absence of AQP4 staining (**Figure 7F-G, Figure S6**).

No differences in AQP4 expression was observed between groups at 24 h post-reperfusion. These results pointed that BBB breakdown took place progressively at a later stage as a consequence of an acute brain damage (**Figure S7**).

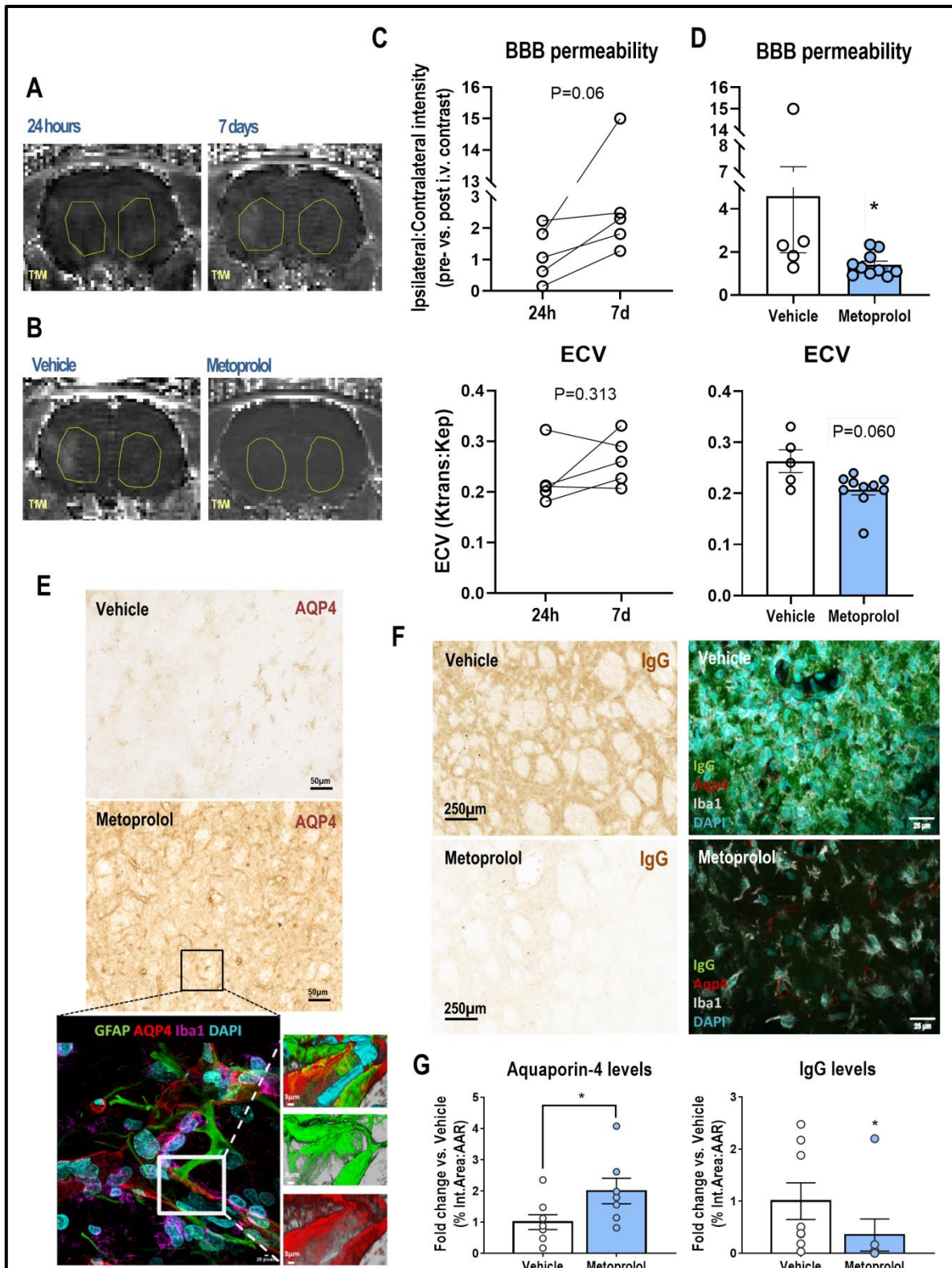


Figure 7. ADRB1 blockade by metoprolol preserves the blood–brain barrier (BBB). (A) Coronal T1-weighted (T1W) MRI at 24 h and 7 d post-reperfusion. (B) Comparative coronal T1W MRI at 7 d post-reperfusion. (C) Loss of BBB permeability at 7 d vs. 24 h post-stroke onset analyzed by comparison of ipsilateral (with infarct) and contralateral (without infarct) intensities in similar-sized areas (yellow outlines), in a single slice per rat on post- vs. pre-contrast T1W MRI and DCE. (D) Quantification of ipsilateral-to-contralateral intensity ratios from post- vs. pre-contrast T1W MRI and DCE images, showing reduced BBB permeability in metoprolol-treated rats (vehicle, n = 5; metoprolol, n = 10). (E) IHC of coronal sections at 7 d post-reperfusion with anti-aquaporin 4 (AQP4) antibody. The bottom panel shows representative triple GFAP+AQP4+Iba1+ immunofluorescence, illustrating AQP4 preservation (red) in astrocyte (GFAP; green) end-feet and consequent preservation of BBB integrity. Microglia/macrophages (Iba1; purple) were found around vessels. Nuclei were revealed with DAPI (blue). (F) IHC of coronal sections at 7 d post-reperfusion with anti-immunoglobulin G (IgG) antibody (left panels). The right panels shows representative triple IgG+AQP4+Iba1+ immunofluorescence, illustrating IgG extravasation (green) in the absence of AQP4 (red). Microglia/macrophages (Iba1; grey) were found more reactive in the core lesion of vehicle-treated rats and nuclei were revealed with DAPI (blue). (G) Quantification of AQP4 and IgG IHC in the MCA of infarcted hemispheres shows preservation of BBB integrity at 7 d post-reperfusion in rats receiving i.v. metoprolol (vehicle, n = 8; metoprolol, n = 7). Graphs show mean \pm S.E.M. *P < 0.05; paired Student t-test (C), or unpaired Mann-Whitney or Student t-test (D, G).

ADRB1 blockade during brain ischemia prevents microglia/macrophage response and reduces sub-acute glial scar formation

In vehicle-injected rats, reactive and hypertrophic astrocytes, detected by upregulated expression of GFAP, accumulated in a barrier pattern surrounding the core lesion and expressed large amounts of CSPGs. Metoprolol injection reduced glial scar formation by 5-fold (vehicle, 1.00 ± 0.18 ; metoprolol, 0.19 ± 0.07 ; $p < 0.01$; **Figure 8A-C, Figure S8A**). In line with this result, proteoglycan production in the core lesion identified by CSPG deposition was reduced by 10-fold in rats receiving i.v. metoprolol (vehicle, 1.00 ± 0.33 ; metoprolol, 0.09 ± 0.04 ; $p < 0.05$; **Figure 8B, 8D, Figure S8A-B**), as well as microglia/macrophage response (vehicle, 1.00 ± 0.17 ; metoprolol, 0.52 ± 0.09 ; $p < 0.05$; **Figure 8A-B, 8E**). Confirming these results, double-ICH and IF for CSPG and GFAP in the vehicle group revealed astrocytes surrounding a scar containing a matrix of proteoglycans, whereas this phenomenon was not seen in metoprolol-treated rats (**Figure S8D**). Moreover, quadruple IF showed that the absence of a glial scar and proteoglycan matrix in the core lesion of metoprolol-treated rats was accompanied by a reduced microglia/macrophage response in the same area (**Figure 5A**), as observed with Iba1 immunohistochemistry (**Figure 8B, 8E**). IHC results at 24 h post-reperfusion indicated that glial scarring was not present in any of the treatment groups. The latter suggests that metoprolol did not have a direct effect on glia (**Figure S5**).

Increased inflammation leads to secondary damage to other cell populations, such as neurons and oligodendrocytes (23). MBP IHC, a marker of the state of axonal myelination, showed good preservation of myelin sheaths in metoprolol treated rats (vehicle, 1.00 ± 0.16 ; metoprolol, 2.02 ± 0.36 ; $p < 0.05$; **Figure 8A-B, 8F, Figure S8C**). Myelin sheaths in the vehicle group showed evidence of damage, and there were large amounts of debris accumulated in the core lesion, coinciding with CSPG deposition (**Figure S8E**). Triple IF confirmed these results, illustrating how

metoprolol injection was associated with better preserved myelin sheaths that resembled those on the contralateral side (**Figure 8A**).

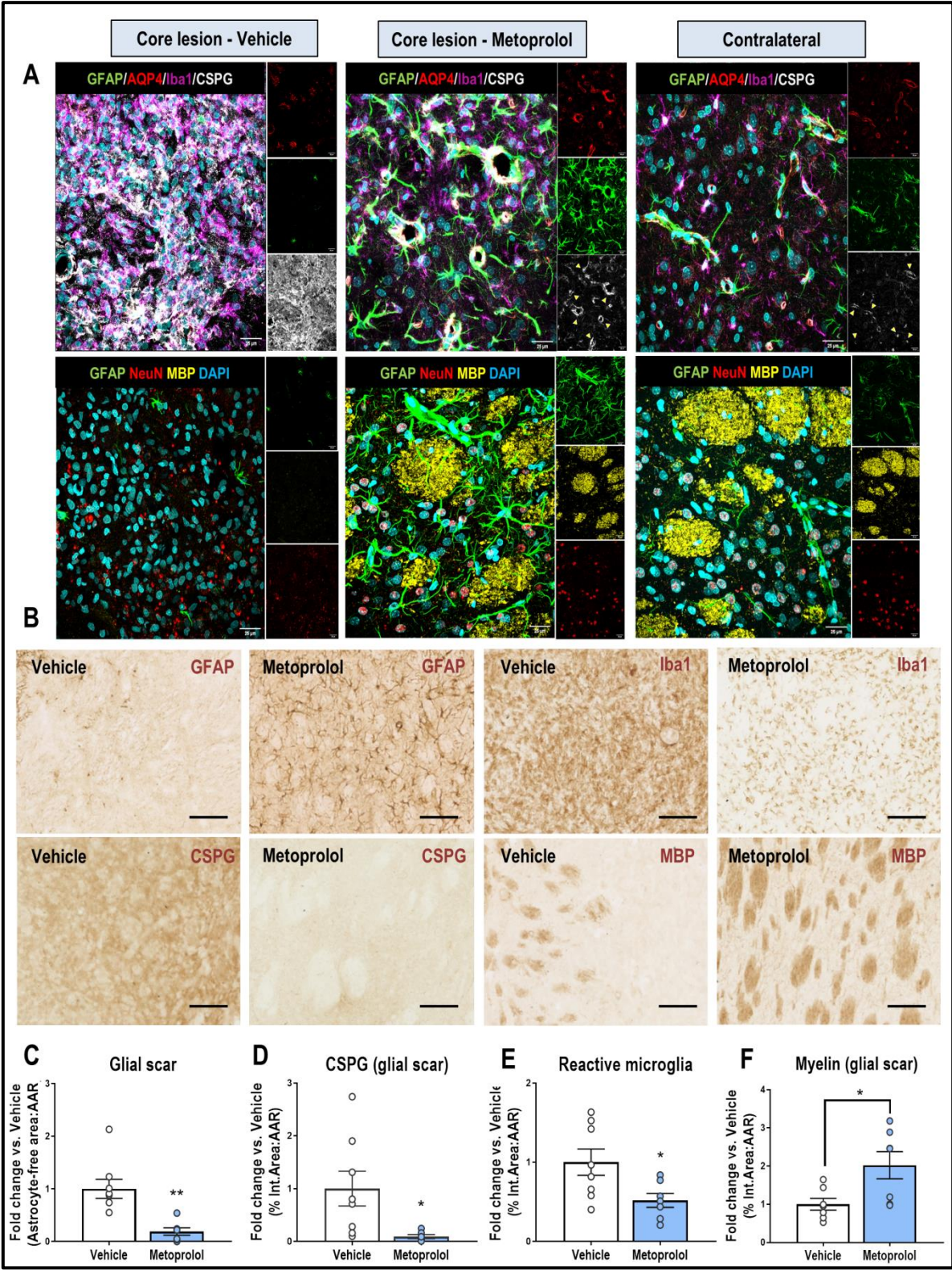


Figure 8. ADRB1 blockade by metoprolol prevents microglia/macrophage response and reduces subacute glial scar formation. (A) Single and merged channels of quadruple GFAP+AQP4+Iba1+CSPG+ (top row) and triple GFAP+MBP+NeuN (bottom row) IF. The quadruple IF shows glial scar formation (GFAP; green), proteoglycan deposition (CSPG; grey), microglia/macrophage response (Iba1; purple), and BBB disruption (AQP4; red) in a vehicle-treated rat (left panels), contrasting the absence of glial scar in a metoprolol-treated rat (central panels). Yellow arrowheads show a suggesting neural/glial antigen 2 expression by CSPG+ perivascular pericytes. The triple IF shows representative degeneration of neurons (NeuN; red) and the myelin sheath (MBP; yellow) in a vehicle-treated rat (left panels) and their preservation in a metoprolol-treated rat (central panels), where the lesion resembles the contralateral hemisphere (right panels) except for the astrocyte hypertrophy (GFAP; green). Nuclei were revealed with DAPI (blue). (B) Representative IHC (vehicle, left panels; metoprolol, right panels) of GFAP (glial fibrillary acidic protein), CSPGs (chondroitin sulfate proteoglycans), Iba1 (ionized calcium-binding adapter molecule 1) and myelin basic protein (MBP) on coronal sections at 7 days post-reperfusion, showing a reduction in glial scar formation (C), proteoglycans deposition (D), reactive microglia response and myelin sheath deterioration in metoprolol-treated rats. n = 6–8 rats per group. Graphs show mean \pm S.E.M. *P < 0.05; unpaired Mann-Whitney or Student t-test. Other abbreviations as in Figure 1.

DISCUSSION

Timely reperfusion is the standard of care for ischemic stroke; however, increasing evidence supports the notion that reperfusion of an ischemic arterial bed induces a secondary form of brain damage, known as reperfusion injury, which leads to BBB dysfunction and HT of the ischemic tissue. Moreover, with the recent advent of endovascular therapy (extending the time window for stroke treatment) (41), I/R injury has become an increasing clinical challenge because there are few interventions able to limit the damage. Neutrophils feature as key protagonists in the proposed mechanisms of cerebral I/R injury, related to their capacity to exacerbate local vascular and tissue injury (45, 54, 55, 64).

Recently, we have reported that selective ADRB1 blockade in neutrophils by metoprolol has a unique and pronounced effect on their activity that results in an amelioration of I/R injury and, consequently, smaller myocardial infarctions (56, 65). We then speculated that a single injection of the β 1-blocker metoprolol might protect the brain during stroke. Even though some studies attributed neuroprotective properties to β -blocker drugs in stroke (66-74), their role has always been controversial and raised debatable discussion. The diversity of β -blocker profiles, routes, and timings of drug administration, as well as the different stroke models and methods for IS and oedema evaluation, has made it difficult to come to a conclusion regarding the use of these agents in stroke outcome. In addition, few mechanisms have been ascribed to this neuroprotection.

Herein, our findings provide strong evidence that the modulating effect of metoprolol on neutrophil dynamics (56) significantly reduces brain injury and promotes inflammatory resolution and tissue repair in a validated model of MCAO/R (75). Metoprolol reduced brain injury and prevented neuronal loss and cerebral oedema progression. This outcome resulted in better preservation of BBB integrity and reduced subacute neuroinflammation.

Since reperfusion therapy is clearly associated with clinical benefits, and given that endovascular thrombectomy has recently extended the reperfusion time window (41), we decided to test a therapy with the potential to reduce reperfusion-related injury in a rodent model of MCAO/R. The non-invasive nature of MRI allowed us to perform a longitudinal analysis of IS at early (day 1) and late (day 7) after reperfusion. This was important because there is uncertainty about the optimal time for IS quantification (76). Additionally, MRI performed during brain ischaemia allowed us to accurately estimate the size of the hypoperfused brain region (AAR) and exclude any influence of anatomical variation on recorded differences between groups (**Figures 4 and S2**). Our results from the MRI study show a robust reduction in brain IS independently of the selected quantification method. Reduction in IS was observed when measured as the AAR-normalized extent of oedema on T2W MRI image, but also when PDM was used to demarcate ischemic penumbra. Comparison of infarct volumes on T2W MRI without normalization also shows that metoprolol-infused rats had significantly smaller infarcts (**Figure 4 and 5**). Histopathology confirms a neuroprotective effect of metoprolol by attenuating neuronal loss in the infarcted brain (**Figure 4**).

Cerebral oedema is a severe complication of ischemic stroke, and medical strategies to reduce its impact are limited (77). DWI is a method of signal contrast generation based on the differences in Brownian motion of water molecules within a voxel of tissue (78). ADC maps show predominantly hypointense and hyperintense areas depending on the restriction to movement of water molecules (79). Therefore, hypointense and hyperintense areas in brain ADC maps are consistent with cytotoxic (cell swelling) and vasogenic oedema (extracellular accumulation of fluid), respectively.

Our results indicate that systemic administration of metoprolol before reperfusion reduces acute cytotoxic and subacute vasogenic oedema (**Figure 6**).

Preservation of BBB integrity is associated with better clearance of toxic cellular by-products, less subsequent permeability and vasogenic oedema, and less secondary neuroinflammation and neuronal death (80). Although DCE-MRI has been widely used to study pathological changes in BBB functionality, studies differ in their MRI procedures and have been performed using a variety of different MRI sequences, contrast agents and time courses. Furthermore, there is no standard method for analyzing the data (81). Here, pre- and post-contrast T1W MRI and DCE suggest BBB breakdown at 7 d, with the ECV increase in the vehicle group indicating a worse BBB integrity as it is reflected by a trend in the K_{trans} and slower contrast washout (lower K_{ep}) (**Figure S5**). Besides, our results from permeability imaging show that early pre-reperfusion i.v. metoprolol preserves BBB structural integrity. These outcomes were consistent with a loss of AQP4 water channels expression at astrocyte end feet in the vehicle-treated group, which was prevented by metoprolol together with a suggesting neural/glial antigen 2 expression by CSPG+ perivascular pericytes (82). BBB integrity preservation by metoprolol was also confirmed by the absence of IgG extravasation (**Figures 7 and S6**). No differences in the BBB state were observed between groups either on MRI or AQP4 expression at 24 h (**Figure 7 and S7**). When evaluating BBB integrity, both MRI and histopathology exhibit a strong correlation, thus pointing that its breakdown took place progressively at a later stage as a consequence of an acute brain damage.

Consistent with all these data, the fact that the rats receiving pre-reperfusion i.v. metoprolol had better long-term behavioral and motor capacities, through a wide range of neurological tests, reinforce and consolidate the translational potential of this therapy as a neuroprotective strategy (**Figure S4**). Although there is abundant experimental evidence that neutrophils play a central role in initiating brain I/R injury, translation to the clinic has so far not yielded clear benefits. The reactive oxygen species scavenger edaravone was found to improve functional outcomes in several clinical trials when administrated within 24 h of stroke onset (83). However, trials testing the ability of agents to block neutrophil–endothelium adhesion failed to improve outcomes (e.g., natalizumab in the ACTION trial (84) and the recombinant protein UK-279,276 in the ASTIN trial (85)). The strategy used in the present study differs from those tested in these earlier trials. Moreover, the anti-neutrophil–endothelium agents in the ACTION and ASTIN trials were initiated after reperfusion, whereas in our study metoprolol was injected during ongoing cerebral ischaemia. The timing of administration seems critical, since MVO occurs immediately upon reperfusion. Intravenous administration of the selective ADRB1 blocker used in this study has been shown to be safe in several clinical trials enrolling acutely ill patients (86), including a recent study showing that its use in COVID-19 patients with acute respiratory distress results in a massive reduction of lung neutrophil infiltration and this translates into less days on mechanical ventilation (87). In addition, metoprolol is easy to administer and inexpensive. Therefore, this study constitutes a largely proof of principle which proposes metoprolol as a strong and promising candidate to be further explored for ischemic stroke treatment.

Study limitations

This study is at the very earliest stages of the translational pathway and therefore presents some limitations that should be addressed in order to translate the potential impact of our findings to the clinics. One of the main limitations is that the study was carried out in young male rats, without including females or any comorbidity such as ageing, hypertension, or diabetes. Moreover, although the MCAO/R model in rodents is one of the most aggressive of ischemic stroke, 35 min of ischaemia is known to cause mild but not severe strokes. To better establish the therapeutic time window of metoprolol, the neuroprotective effect of its administration should be explored at different times of cerebral ischemia and upon (or early after) reperfusion. In addition, testing pre-reperfusion i.v. metoprolol in a stroke model of longer time of ischemia (≈ 90 min) could be also interesting to be considered before translation to clinics.

CONCLUSIONS

1. Selective ADRB1 blockade by i.v. metoprolol administration during ongoing ischemic stroke exerts a neuroprotective effect by reducing IS and neuronal loss, and improving neurological outcomes. Reduction in brain IS by metoprolol is independent of the selected MRI quantification method.
2. Brain acute cytotoxic and subacute vasogenic oedema was reduced by i.v. metoprolol at 24 h and 7 d post-reperfusion, respectively. Attenuation of vasogenic oedema is consistent with the preservation of the BBB integrity by metoprolol at day 7. Both permeability imaging and histopathological analyses exhibit a strong correlation when assessing the BBB state.
3. Histopathological analysis shows that i.v. administration of metoprolol before reperfusion prevents microglia/macrophage response, loss of myelin sheaths and reduces subacute glial scar formation, proteoglycan deposition and thus neuroinflammation.

Author contributions

Part of the present work has been published as an original investigation in the British Journal of Pharmacology in which the contribution was as first-author:

Clemente-Moragón A, Oliver E, Calle D, Cussó L, Gómez M, Pradillo JM, Castejón R, Rallón N, Benito JM, Fernández-Ferro JC, Carneado-Ruíz J, Moro MA, Sánchez-González J, Fuster V, Cortés-Canteli M, Desco M, Ibáñez B. **Neutrophil β 1 adrenoceptor blockade blunts stroke-associated neuroinflammation.** Br J Pharmacol. 2023;180(4):459-478. doi: 10.1111/bph.15963. PMID: 36181002.

The present TCI focuses on the evaluation of different features of brain ischemia/reperfusion injury (infarct size, oedema and blood-brain-barrier integrity) and the impact of new neuroprotective strategies (i.v. metoprolol) by MRI. Whether MRI findings were consistent with results from histopathology (immunohistochemistry and immunofluorescence) analyses was also assessed. The contribution of the author to this work was as follows:

- Design of the entire study.
- Overall MRI analyses (quantification of infarct size, area-at-risk, cytotoxic and vasogenic oedema and blood-brain-barrier integrity).
- Hemodynamic dose-response study.
- Tissue processing, immunostaining experiments and immunohistochemical analyses.
- Statistical analyses, interpretation of results and manuscript writing.

Acknowledgements

I would like to thank everyone implicated in the publication in the British Journal of Pharmacology (Clemente-Moragón A, et al. 2023), particularly to Borja Ibáñez, Javier Sánchez, Eduardo Oliver, Marta Cortés, María Ángeles Moro and Manuel Desco. I also thank Alexandra de Francisco, Yolanda Sierra and María de la Jara-Felipe for their project involvement and great skills with surgical procedures in rats. We also thank Lucía López Palomar for her help collecting and fixing brains, Ana Marcos for sharing her expertise with brain tissue processing and Verónica Labrador for her command with microscopy image capture and video editing. We thank Antonio de Molina for his support with the histopathological analysis. Simon Bartlett (CNIC) provided English editing.

Funding

This study received funding from the Instituto de Salud Carlos III (ISCIII; PI16/02110 to B.I and PT20/00044 to MD), the European Regional Development Fund (ERDF) "A way of making Europe", the Comunidad de Madrid (S2017/BMD-3867 RENIM-CM to MD and BI) cofunded with European structural and investment funds and by Agencia Estatal de Investigación (PID2019-110369RB-I00 to B.I). BI is a recipient of funding from the European Research Council (ERC) under the European Union Horizon 2020 Research and Innovation Programme (ERC-Consolidator

Grant agreement No. 819775). EO is a recipient of funds from the Comunidad de Madrid Programa de Atracción de Talento (2017-T1/BMD-5185) and from a Ramón y Cajal grant (RYC2020-028884-I) funded by MCIN/AEI/ 10.13039/501100011033 and by “ESF Investing in your future”. ACM is the beneficiary of an FPU fellowship from the Ministerio de Ciencia e Innovación (FPU2017/01932). MCC is the beneficiary of a Miguel Servet contract (MS16/00174). The CNIC is supported by the ISCIII, the Ministerio de Ciencia e Innovación and the Pro CNIC Foundation and is a Severo Ochoa Center of Excellence (CEX2020-001041-S).

BIBLIOGRAPHY

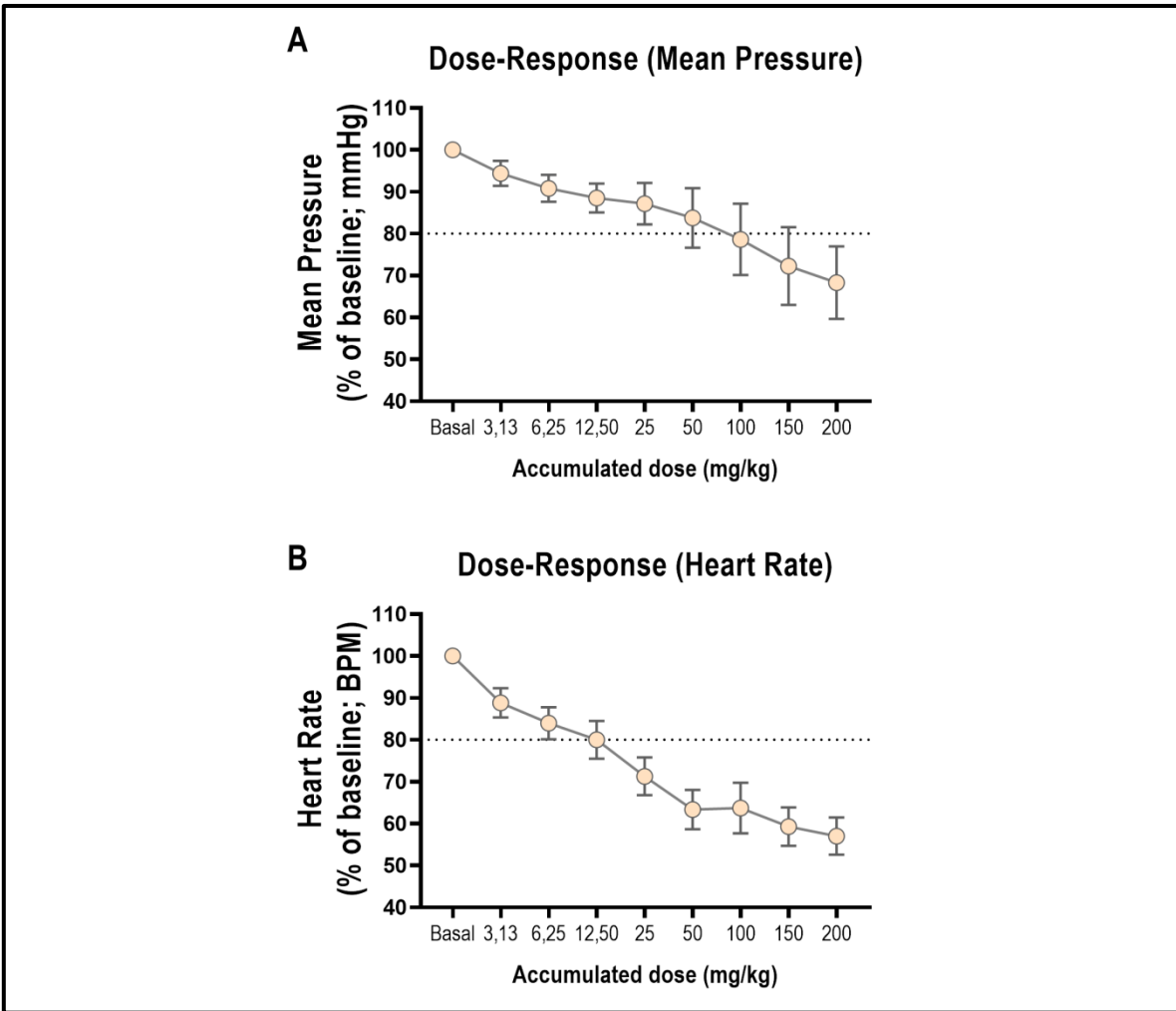
1. Campbell BCV, De Silva DA, Macleod MR, Coutts SB, Schwamm LH, Davis SM, et al. Ischaemic stroke. *Nature reviews Disease primers*. 2019;5(1):70.
2. Hu X, De Silva TM, Chen J, Faraci FM. Cerebral Vascular Disease and Neurovascular Injury in Ischemic Stroke. *Circulation research*. 2017;120(3):449-71.
3. Patil S, Rossi R, Jabrah D, Doyle K. Detection, Diagnosis and Treatment of Acute Ischemic Stroke: Current and Future Perspectives. *Frontiers in medical technology*. 2022;4:748949.
4. Rai AT, Seldon AE, Boo S, Link PS, Domico JR, Tarabishy AR, et al. A population-based incidence of acute large vessel occlusions and thrombectomy eligible patients indicates significant potential for growth of endovascular stroke therapy in the USA. *Journal of neurointerventional surgery*. 2017;9(8):722-6.
5. Heit JJ, Sussman ES, Wintermark M. Perfusion Computed Tomography in Acute Ischemic Stroke. *Radiologic clinics of North America*. 2019;57(6):1109-16.
6. Powers WJ, Rabinstein AA, Ackerson T, Adeoye OM, Bambakidis NC, Becker K, et al. Guidelines for the Early Management of Patients With Acute Ischemic Stroke: 2019 Update to the 2018 Guidelines for the Early Management of Acute Ischemic Stroke: A Guideline for Healthcare Professionals From the American Heart Association/American Stroke Association. *Stroke*. 2019;50(12):e344-e418.
7. Berkhemer OA, Fransen PS, Beumer D, van den Berg LA, Lingsma HF, Yoo AJ, et al. A randomized trial of intraarterial treatment for acute ischemic stroke. *The New England journal of medicine*. 2015;372(1):11-20.
8. Campbell BC, Mitchell PJ, Investigators E-I. Endovascular therapy for ischemic stroke. *The New England journal of medicine*. 2015;372(24):2365-6.
9. Albers GW, Marks MP, Kemp S, Christensen S, Tsai JP, Ortega-Gutierrez S, et al. Thrombectomy for Stroke at 6 to 16 Hours with Selection by Perfusion Imaging. *The New England journal of medicine*. 2018;378(8):708-18.
10. Yew KS, Cheng E. Acute stroke diagnosis. *American family physician*. 2009;80(1):33-40.
11. Schaefer PW, Grant PE, Gonzalez RG. Diffusion-weighted MR imaging of the brain. *Radiology*. 2000;217(2):331-45.
12. Mullins ME, Schaefer PW, Sorensen AG, Halpern EF, Ay H, He J, et al. CT and conventional and diffusion-weighted MR imaging in acute stroke: study in 691 patients at presentation to the emergency department. *Radiology*. 2002;224(2):353-60.
13. Currie S, Hoggard N, Craven IJ, Hadjivassiliou M, Wilkinson ID. Understanding MRI: basic MR physics for physicians. *Postgraduate medical journal*. 2013;89(1050):209-23.
14. Provost C, Soudant M, Legrand L, Ben Hassen W, Xie Y, Soize S, et al. Magnetic Resonance Imaging or Computed Tomography Before Treatment in Acute Ischemic Stroke. *Stroke*. 2019;50(3):659-64.
15. Vymazal J, Rulseh AM, Keller J, Janouskova L. Comparison of CT and MR imaging in ischemic stroke. *Insights into imaging*. 2012;3(6):619-27.
16. Birenbaum D, Bancroft LW, Felsberg GJ. Imaging in acute stroke. *The western journal of emergency medicine*. 2011;12(1):67-76.
17. Hall RA. Beta-adrenergic receptors and their interacting proteins. *Seminars in cell & developmental biology*. 2004;15(3):281-8.
18. Alexander SP, Christopoulos A, Davenport AP, Kelly E, Mathie A, Peters JA, et al. THE CONCISE GUIDE TO PHARMACOLOGY 2021/22: G protein-coupled receptors. *British journal of pharmacology*. 2021;178 Suppl 1:S27-S156.
19. de Lucia C, Eguchi A, Koch WJ. New Insights in Cardiac beta-Adrenergic Signaling During Heart Failure and Aging. *Frontiers in pharmacology*. 2018;9:904.
20. Warne T, Serrano-Vega MJ, Baker JG, Moukhametzianov R, Edwards PC, Henderson R, et al. Structure of a beta1-adrenergic G-protein-coupled receptor. *Nature*. 2008;454(7203):486-91.
21. Warne T, Moukhametzianov R, Baker JG, Nehme R, Edwards PC, Leslie AG, et al. The structural basis for agonist and partial agonist action on a beta(1)-adrenergic receptor. *Nature*. 2011;469(7329):241-4.
22. Kobilka BK. Structural insights into adrenergic receptor function and pharmacology. *Trends in pharmacological sciences*. 2011;32(4):213-8.
23. Baker JG. The selectivity of beta-adrenoceptor antagonists at the human beta1, beta2 and beta3 adrenoceptors. *British journal of pharmacology*. 2005;144(3):317-22.
24. Baker JG. Site of action of beta-ligands at the human beta1-adrenoceptor. *The Journal of pharmacology and experimental therapeutics*. 2005;313(3):1163-71.
25. Baker JG. Evidence for a secondary state of the human beta3-adrenoceptor. *Molecular pharmacology*. 2005;68(6):1645-55.

26. Lopez-Sendon J, Swedberg K, McMurray J, Tamargo J, Maggioni AP, Dargie H, et al. Expert consensus document on beta-adrenergic receptor blockers. *European heart journal*. 2004;25(15):1341-62.
27. Pott C, Brixius K, Bundkirchen A, Bolck B, Bloch W, Steinritz D, et al. The preferential beta3-adrenoceptor agonist BRL 37344 increases force via beta1-/beta2-adrenoceptors and induces endothelial nitric oxide synthase via beta3-adrenoceptors in human atrial myocardium. *British journal of pharmacology*. 2003;138(3):521-9.
28. Pott C, Steinritz D, Napp A, Bloch W, Schwinger RH, Brixius K. [On the function of beta3-adrenoceptors in the human heart: signal transduction, inotropic effect and therapeutic prospects]. *Wiener medizinische Wochenschrift*. 2006;156(15-16):451-8.
29. Weber MA. The role of the new beta-blockers in treating cardiovascular disease. *American journal of hypertension*. 2005;18(12 Pt 2):169S-76S.
30. Ladage D, Schwinger RH, Brixius K. Cardio-selective beta-blocker: pharmacological evidence and their influence on exercise capacity. *Cardiovascular therapeutics*. 2013;31(2):76-83.
31. do Vale GT, Ceron CS, Gonzaga NA, Simplicio JA, Padovan JC. Three Generations of beta-blockers: History, Class Differences and Clinical Applicability. *Current hypertension reviews*. 2019;15(1):22-31.
32. Brunton LL LJ, Parker KL. Goodman & Gilman: Las bases farmacológicas de la terapéutica. McGrawHill. 6th Chapter2006 (11th Edition). p. 237-95.
33. Ibanez B, Prat-Gonzalez S, Speidl WS, Vilahur G, Pinero A, Cimmino G, et al. Early metoprolol administration before coronary reperfusion results in increased myocardial salvage: analysis of ischemic myocardium at risk using cardiac magnetic resonance. *Circulation*. 2007;115(23):2909-16.
34. Ibanez B, Cimmino G, Prat-Gonzalez S, Vilahur G, Hutter R, Garcia MJ, et al. The cardioprotection granted by metoprolol is restricted to its administration prior to coronary reperfusion. *International journal of cardiology*. 2011;147(3):428-32.
35. Ibanez B, Macaya C, Sanchez-Brunete V, Pizarro G, Fernandez-Friera L, Mateos A, et al. Effect of early metoprolol on infarct size in ST-segment-elevation myocardial infarction patients undergoing primary percutaneous coronary intervention: the Effect of Metoprolol in Cardioprotection During an Acute Myocardial Infarction (METOCARD-CNIC) trial. *Circulation*. 2013;128(14):1495-503.
36. Pizarro G, Fernandez-Friera L, Fuster V, Fernandez-Jimenez R, Garcia-Ruiz JM, Garcia-Alvarez A, et al. Long-term benefit of early pre-reperfusion metoprolol administration in patients with acute myocardial infarction: results from the METOCARD-CNIC trial (Effect of Metoprolol in Cardioprotection During an Acute Myocardial Infarction). *Journal of the American College of Cardiology*. 2014;63(22):2356-62.
37. Diaz-Munoz R, Valle-Caballero MJ, Sanchez-Gonzalez J, Pizarro G, Garcia-Rubira JC, Escalera N, et al. Intravenous metoprolol during ongoing STEMI ameliorates markers of ischemic injury: a METOCARD-CNIC trial electrocardiographic study. *Basic research in cardiology*. 2021;116(1):45.
38. Garcia-Ruiz JM, Fernandez-Jimenez R, Garcia-Alvarez A, Pizarro G, Galan-Arriola C, Fernandez-Friera L, et al. Impact of the Timing of Metoprolol Administration During STEMI on Infarct Size and Ventricular Function. *Journal of the American College of Cardiology*. 2016;67(18):2093-104.
39. Lobo-Gonzalez M, Galan-Arriola C, Rossello X, Gonzalez-Del-Hoyo M, Vilchez JP, Higuero-Verdejo MI, et al. Metoprolol blunts the time-dependent progression of infarct size. *Basic research in cardiology*. 2020;115(5):55.
40. Dai X, Kaul P, Smith SC, Jr., Stouffer GA. Predictors, treatment, and outcomes of STEMI occurring in hospitalized patients. *Nature reviews Cardiology*. 2016;13(3):148-54.
41. Nogueira RG, Jadhav AP, Haussen DC, Bonafe A, Budzik RF, Bhuva P, et al. Thrombectomy 6 to 24 Hours after Stroke with a Mismatch between Deficit and Infarct. *The New England journal of medicine*. 2018;378(1):11-21.
42. Ibanez B, Heusch G, Ovize M, Van de Werf F. Evolving therapies for myocardial ischemia/reperfusion injury. *Journal of the American College of Cardiology*. 2015;65(14):1454-71.
43. Garcia-Dorado D, Ruiz-Meana M, Piper HM. Lethal reperfusion injury in acute myocardial infarction: facts and unresolved issues. *Cardiovascular research*. 2009;83(2):165-8.
44. Eltzschig HK, Eckle T. Ischemia and reperfusion--from mechanism to translation. *Nature medicine*. 2011;17(11):1391-401.
45. L L, X W, Z Y. Ischemia-reperfusion Injury in the Brain: Mechanisms and Potential Therapeutic Strategies. *Biochemistry & pharmacology* : open access. 2016;5(4).

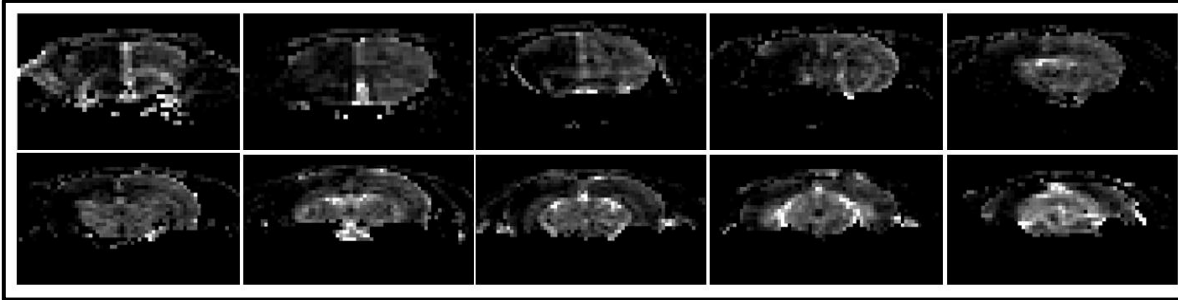
46. Enzmann G, Kargaran S, Engelhardt B. Ischemia-reperfusion injury in stroke: impact of the brain barriers and brain immune privilege on neutrophil function. *Therapeutic advances in neurological disorders*. 2018;11:1756286418794184.
47. Sanz-Rosa D, Garcia-Prieto J, Ibanez B. The future: therapy of myocardial protection. *Annals of the New York Academy of Sciences*. 2012;1254:90-8.
48. Kloner RA, King KS, Harrington MG. No-reflow phenomenon in the heart and brain. *American journal of physiology Heart and circulatory physiology*. 2018;315(3):H550-H62.
49. Heusch G. The Coronary Circulation as a Target of Cardioprotection. *Circulation research*. 2016;118(10):1643-58.
50. Heusch G. Coronary microvascular obstruction: the new frontier in cardioprotection. *Basic research in cardiology*. 2019;114(6):45.
51. Vinten-Johansen J. Involvement of neutrophils in the pathogenesis of lethal myocardial reperfusion injury. *Cardiovascular research*. 2004;61(3):481-97.
52. Sreeramkumar V, Adrover JM, Ballesteros I, Cuartero MI, Rossaint J, Bilbao I, et al. Neutrophils scan for activated platelets to initiate inflammation. *Science*. 2014;346(6214):1234-8.
53. Fernandez-Jimenez R, Garcia-Prieto J, Sanchez-Gonzalez J, Agüero J, Lopez-Martin GJ, Galan-Arriola C, et al. Pathophysiology Underlying the Bimodal Edema Phenomenon After Myocardial Ischemia/Reperfusion. *Journal of the American College of Cardiology*. 2015;66(7):816-28.
54. Jickling GC, Liu D, Ander BP, Stamova B, Zhan X, Sharp FR. Targeting neutrophils in ischemic stroke: translational insights from experimental studies. *Journal of cerebral blood flow and metabolism : official journal of the International Society of Cerebral Blood Flow and Metabolism*. 2015;35(6):888-901.
55. Strecker JK, Schmidt A, Schabitz WR, Minnerup J. Neutrophil granulocytes in cerebral ischemia - Evolution from killers to key players. *Neurochemistry international*. 2017;107:117-26.
56. Garcia-Prieto J, Villena-Gutierrez R, Gomez M, Bernardo E, Pun-Garcia A, Garcia-Lunar I, et al. Neutrophil stunning by metoprolol reduces infarct size. *Nature communications*. 2017;8:14780.
57. Tofts PS, Brix G, Buckley DL, Evelhoch JL, Henderson E, Knopp MV, et al. Estimating kinetic parameters from dynamic contrast-enhanced T(1)-weighted MRI of a diffusable tracer: standardized quantities and symbols. *Journal of magnetic resonance imaging : JMRI*. 1999;10(3):223-32.
58. Butcher K, Parsons M, Allport L, Lee SB, Barber PA, Tress B, et al. Rapid assessment of perfusion-diffusion mismatch. *Stroke*. 2008;39(1):75-81.
59. Paxinos G. *The Rat Brain in Stereotaxic Coordinates*. Elsevier Inc. 2007;6th Edition.
60. Popp A, Jaenisch N, Witte OW, Frahm C. Identification of ischemic regions in a rat model of stroke. *PloS one*. 2009;4(3):e4764.
61. Tamura A, Graham DI, McCulloch J, Teasdale GM. Focal cerebral ischaemia in the rat: 1. Description of technique and early neuropathological consequences following middle cerebral artery occlusion. *Journal of cerebral blood flow and metabolism : official journal of the International Society of Cerebral Blood Flow and Metabolism*. 1981;1(1):53-60.
62. Cortes-Canteli M, Luna-Medina R, Sanz-Sancristobal M, Alvarez-Barrientos A, Santos A, Perez-Castillo A. CCAAT/enhancer binding protein beta deficiency provides cerebral protection following excitotoxic injury. *Journal of cell science*. 2008;121(Pt 8):1224-34.
63. Fukuda AM, Badaut J. Aquaporin 4: a player in cerebral edema and neuroinflammation. *Journal of neuroinflammation*. 2012;9:279.
64. Kolaczowska E, Kubes P. Neutrophil recruitment and function in health and inflammation. *Nature reviews Immunology*. 2013;13(3):159-75.
65. Clemente-Moragon A, Gomez M, Villena-Gutierrez R, Lalama DV, Garcia-Prieto J, Martinez F, et al. Metoprolol exerts a non-class effect against ischaemia-reperfusion injury by abrogating exacerbated inflammation. *European heart journal*. 2020;41(46):4425-40.
66. Ajmo CT, Jr., Collier LA, Leonardo CC, Hall AA, Green SM, Womble TA, et al. Blockade of adrenoceptors inhibits the splenic response to stroke. *Experimental neurology*. 2009;218(1):47-55.
67. Goyagi T, Kimura T, Nishikawa T, Tobe Y, Masaki Y. Beta-adrenoreceptor antagonists attenuate brain injury after transient focal ischemia in rats. *Anesthesia and analgesia*. 2006;103(3):658-63.
68. Goyagi T, Horiguchi T, Nishikawa T, Tobe Y. Post-treatment with selective beta1 adrenoceptor antagonists provides neuroprotection against transient focal ischemia in rats. *Brain research*. 2010;1343:213-7.

69. Goyagi T, Nishikawa T, Tobe Y. Neuroprotective effects and suppression of ischemia-induced glutamate elevation by beta1-adrenoreceptor antagonists administered before transient focal ischemia in rats. *Journal of neurosurgical anesthesiology*. 2011;23(2):131-7.
70. Gui H, Guo YF, Liu X, Zhang JM, Yang YL, Huang GZ, et al. Effects of combination therapy with levamlodipine and bisoprolol on stroke in rats. *CNS neuroscience & therapeutics*. 2013;19(3):178-82.
71. Hertz L, Xu J, Chen Y, Gibbs ME, Du T, Hertz L, et al. Antagonists of the Vasopressin V1 Receptor and of the beta(1)-Adrenoceptor Inhibit Cytotoxic Brain Edema in Stroke by Effects on Astrocytes - but the Mechanisms Differ. *Current neuropharmacology*. 2014;12(4):308-23.
72. Iwata M, Inoue S, Kawaguchi M, Nakamura M, Konishi N, Furuya H. Posttreatment but not pretreatment with selective beta-adrenoreceptor 1 antagonists provides neuroprotection in the hippocampus in rats subjected to transient forebrain ischemia. *Anesthesia and analgesia*. 2010;110(4):1126-32.
73. Little JR, Latchaw JP, Jr., Slugg RM, Lesser RP, Stowe NT. Treatment of acute focal cerebral ischemia with propranolol. *Stroke*. 1982;13(3):302-7.
74. Savitz SI, Erhardt JA, Anthony JV, Gupta G, Li X, Barone FC, et al. The novel beta-blocker, carvedilol, provides neuroprotection in transient focal stroke. *Journal of cerebral blood flow and metabolism : official journal of the International Society of Cerebral Blood Flow and Metabolism*. 2000;20(8):1197-204.
75. Cai Q, Xu G, Liu J, Wang L, Deng G, Liu J, et al. A modification of intraluminal middle cerebral artery occlusion/reperfusion model for ischemic stroke with laser Doppler flowmetry guidance in mice. *Neuropsychiatric disease and treatment*. 2016;12:2851-8.
76. Neumann-Haefelin T, Kastrup A, de Crespigny A, Yenari MA, Ringer T, Sun GH, et al. Serial MRI after transient focal cerebral ischemia in rats: dynamics of tissue injury, blood-brain barrier damage, and edema formation. *Stroke*. 2000;31(8):1965-72; discussion 72-3.
77. Thoren M, Azevedo E, Dawson J, Egidio JA, Falcou A, Ford GA, et al. Predictors for Cerebral Edema in Acute Ischemic Stroke Treated With Intravenous Thrombolysis. *Stroke*. 2017;48(9):2464-71.
78. Baliyan V, Das CJ, Sharma R, Gupta AK. Diffusion weighted imaging: Technique and applications. *World journal of radiology*. 2016;8(9):785-98.
79. Koch S, Rabinstein A, Falcone S, Forteza A. Diffusion-weighted imaging shows cytotoxic and vasogenic edema in eclampsia. *AJNR American journal of neuroradiology*. 2001;22(6):1068-70.
80. Abdullahi W, Tripathi D, Ronaldson PT. Blood-brain barrier dysfunction in ischemic stroke: targeting tight junctions and transporters for vascular protection. *American journal of physiology Cell physiology*. 2018;315(3):C343-C56.
81. Heye AK, Culling RD, Valdes Hernandez Mdel C, Thrippleton MJ, Wardlaw JM. Assessment of blood-brain barrier disruption using dynamic contrast-enhanced MRI. A systematic review. *NeuroImage Clinical*. 2014;6:262-74.
82. Sharif Y, Jumah F, Coplan L, Krosser A, Sharif K, Tubbs RS. Blood brain barrier: A review of its anatomy and physiology in health and disease. *Clinical anatomy*. 2018;31(6):812-23.
83. Enomoto M, Endo A, Yatsushige H, Fushimi K, Otomo Y. Clinical Effects of Early Edaravone Use in Acute Ischemic Stroke Patients Treated by Endovascular Reperfusion Therapy. *Stroke*. 2019;50(3):652-8.
84. Elkins J, Veltkamp R, Montaner J, Johnston SC, Singhal AB, Becker K, et al. Safety and efficacy of natalizumab in patients with acute ischaemic stroke (ACTION): a randomised, placebo-controlled, double-blind phase 2 trial. *The Lancet Neurology*. 2017;16(3):217-26.
85. Krams M, Lees KR, Hacke W, Grieve AP, Orgogozo JM, Ford GA, et al. Acute Stroke Therapy by Inhibition of Neutrophils (ASTIN): an adaptive dose-response study of UK-279,276 in acute ischemic stroke. *Stroke*. 2003;34(11):2543-8.
86. Chatterjee S, Chaudhuri D, Vedanthan R, Fuster V, Ibanez B, Bangalore S, et al. Early intravenous beta-blockers in patients with acute coronary syndrome--a meta-analysis of randomized trials. *International journal of cardiology*. 2013;168(2):915-21.
87. Clemente-Moragon A, Martinez-Milla J, Oliver E, Santos A, Flandes J, Fernandez I, et al. Metoprolol in Critically Ill Patients With COVID-19. *Journal of the American College of Cardiology*. 2021;78(10):1001-11.

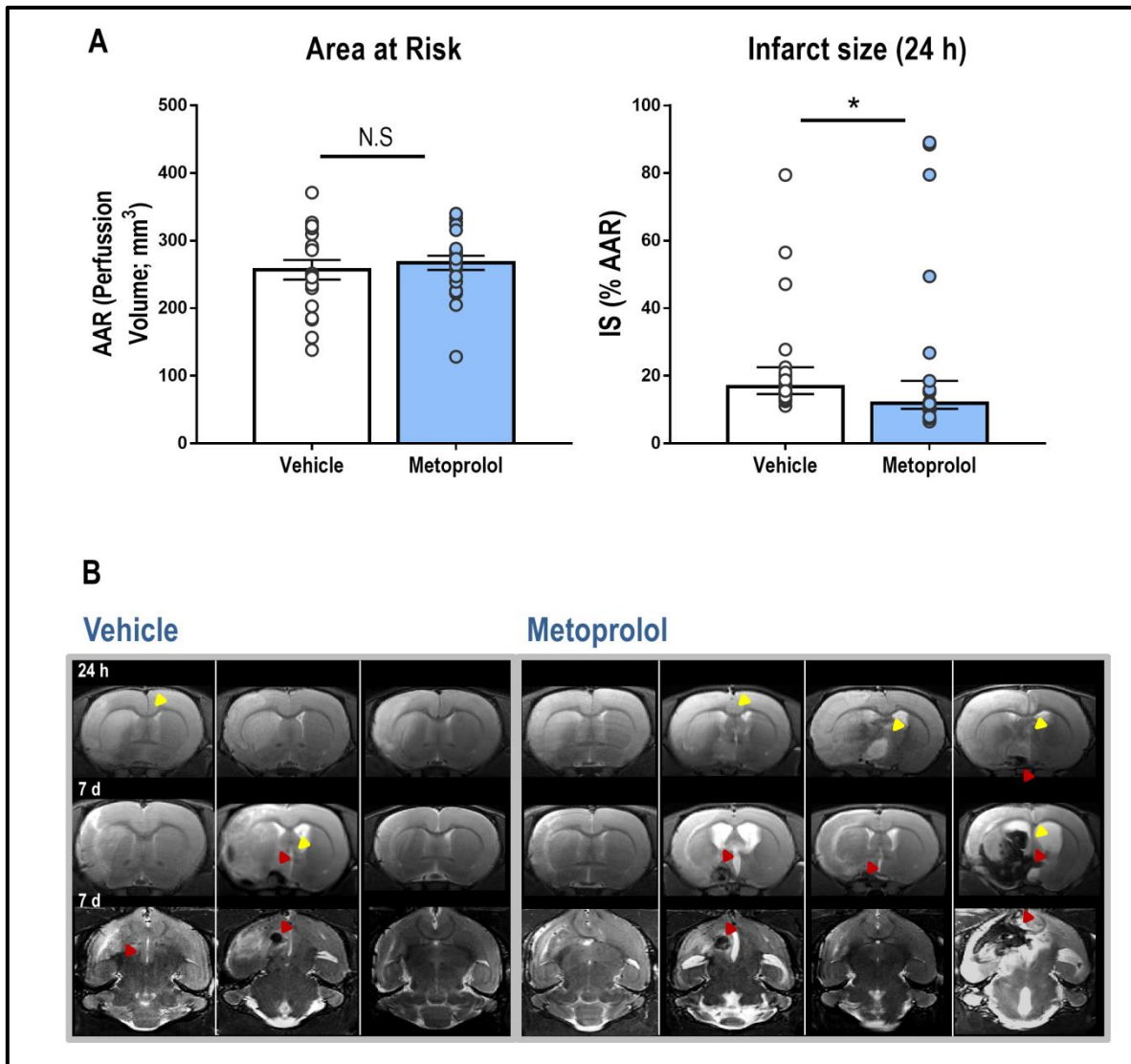
APPENDIX



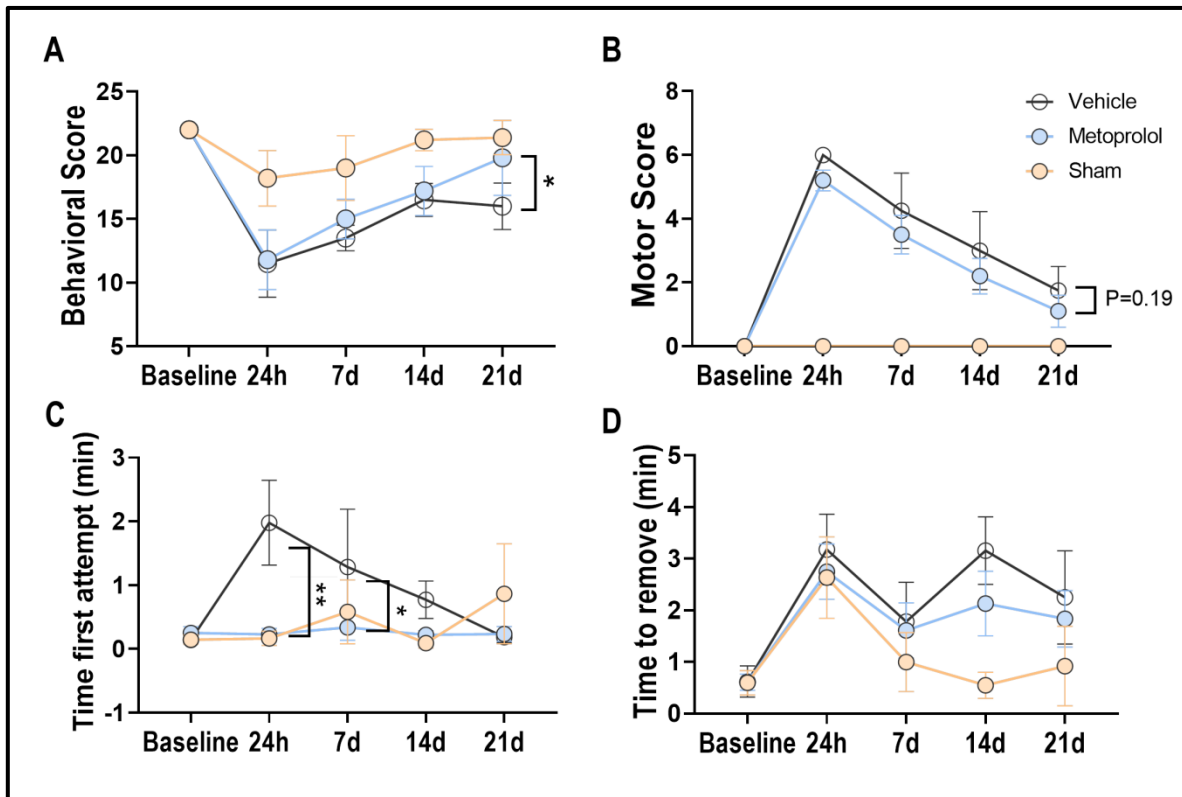
Supplemental Figure 1. The hemodynamic study of 8 different doses of metoprolol (3.13, 6.25, 12.5, the formerly chosen dose, 25, 50, 100, 150 and 200 mg/Kg). Intravenous 12.5 mg/kg dose of metoprolol induced a moderate hemodynamic effect, as indicated by decrease in arterial pressure (mmHg) (**A**) and heart rate (bpm) (**B**) of less than 20%. These data support the selection of 12.5 mg/Kg i.v. injection for the experimental model of ischemic stroke. n=5 animals.



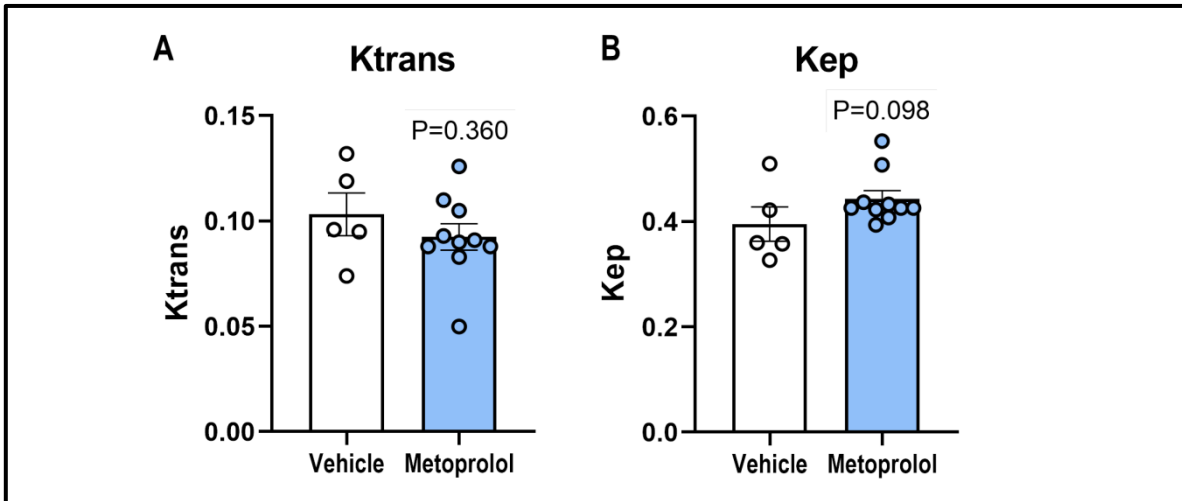
Supplemental Figure 2. The extent of cerebral ischemia provoked by middle cerebral artery occlusion (area at risk, AAR) was determined from MRI dynamic susceptibility contrast (DSC) images obtained during occlusion, and did not differ between groups (see also Figure 4).



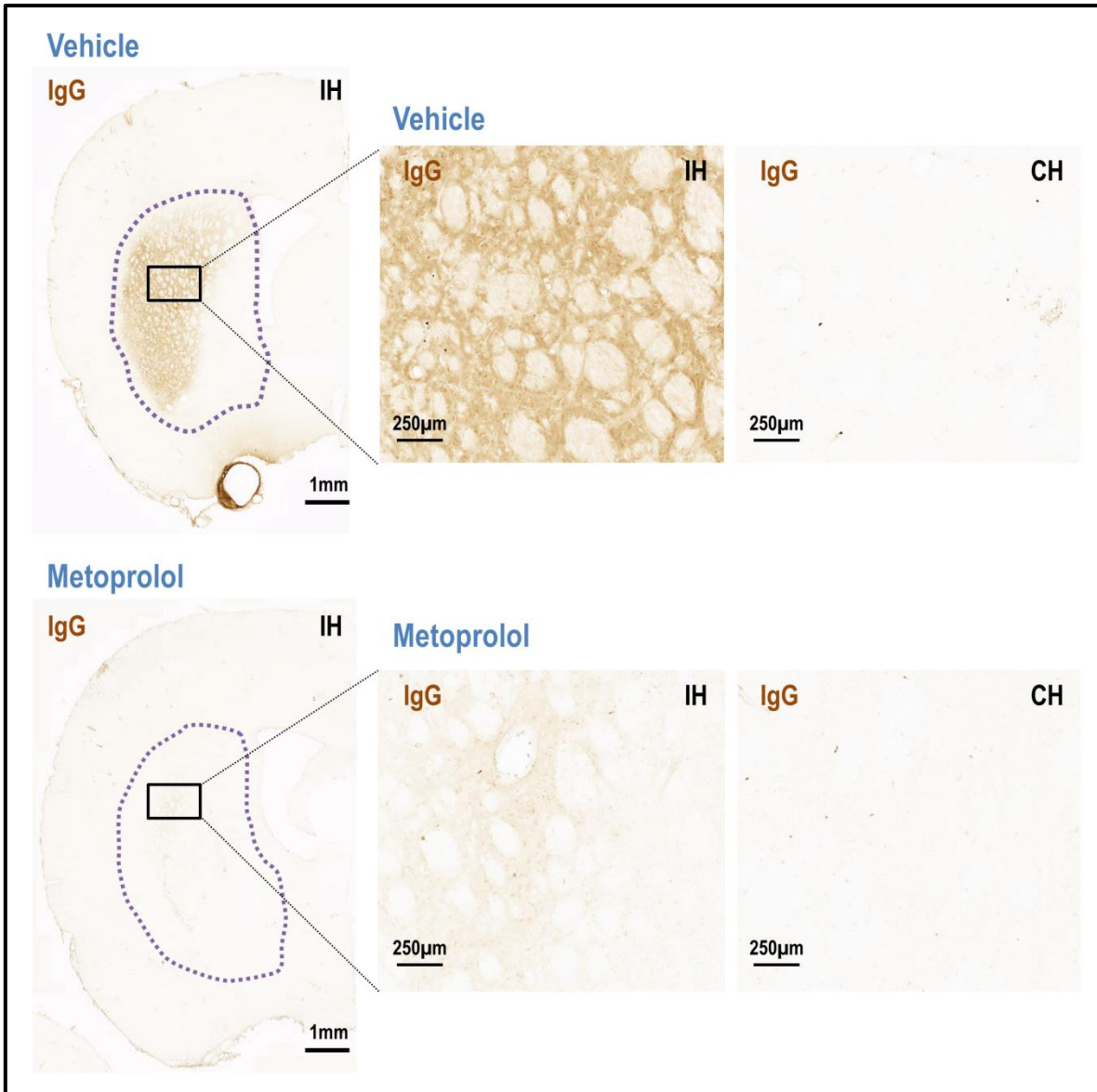
Supplemental Figure 3. (A) Area at risk (AAR), determined by dynamic susceptibility contrast perfusion imaging, and infarct size assessed by coronal T2-weighted (T2W) MRI at 24 h post-reperfusion (vehicle, n=19; metoprolol, n=23). Infarct size was calculated as the ratio of infarct volume to the AAR and expressed as a percentage. After inclusion of all rats in the statistical analysis (including those with IS > 40%), the significant difference ($p < 0.05$) was maintained between rats receiving pre-reperfusion vehicle or metoprolol. Dots correspond to individual rats, column heights to median values, and whiskers to interquartile range. * $p < 0.05$; unpaired Mann-Whitney test. (B) T2W MRI at 24 h post-reperfusion (top row; coronal plane) and 7 d post-reperfusion (middle and bottom rows; coronal and axial planes, respectively) in vehicle-treated rats (left) and metoprolol-treated rats (right) with IS >40%. Infarct regions correspond to hyperintense areas. Rats with IS >40% also showed a midline shift (yellow arrowheads) or hemorrhage (red arrowheads) at 7 d post-reperfusion.



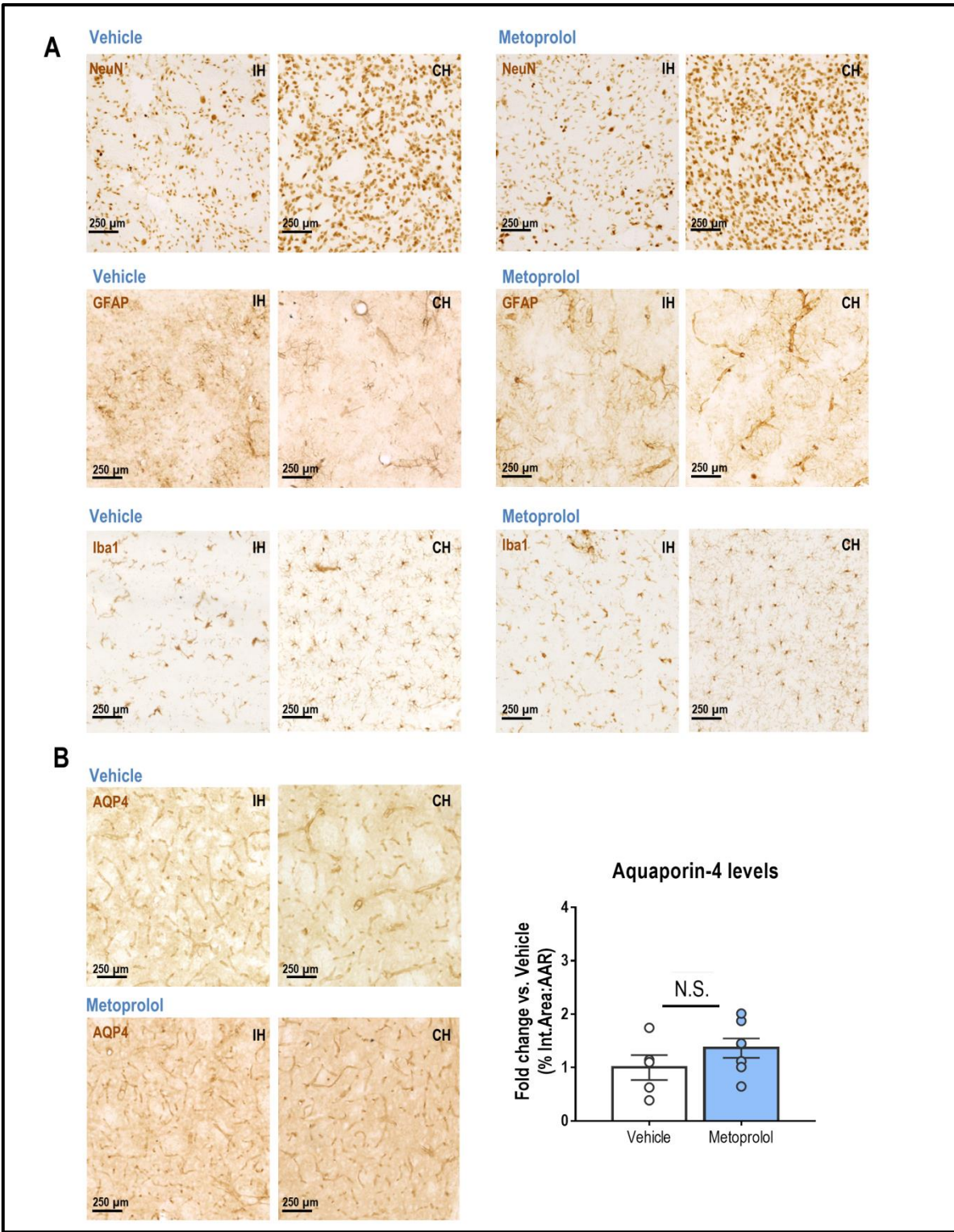
Supplemental Figure 4. A longitudinal study was performed to evaluate long-term effects of brain injury on sensory-motor behaviors. The results obtained with the behavioral (A) and motor (B) scales showed a better neurological function in the metoprolol-treated group. Our evaluation of the sensorimotor functions using the adhesive removal test also revealed an improvement in these neurological deficits (C, D) in the parameter of time for the first attempt to remove the adhesive (C). Sham, n=5; vehicle, n=5; metoprolol, n=10; 1 rat excluded upon confirmation of the absence of artery occlusion. Data are means \pm S.E.M. * p <0.05, ** p <0.01; unpaired Mann-Whitney or Student t-test.



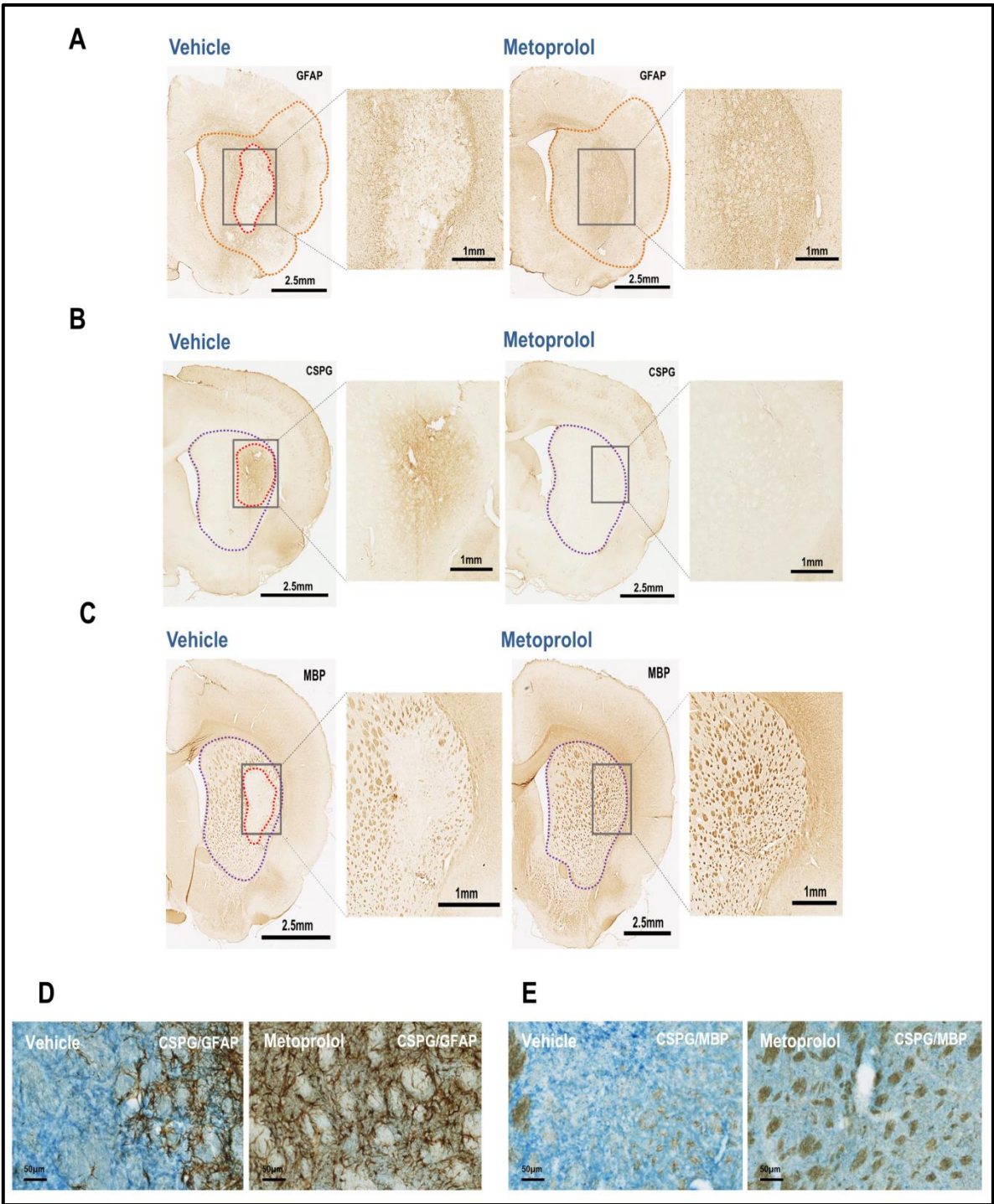
Supplemental Figure 5. Analysis of DCE images revealing attenuation in BBB permeability (Ktrans) (**A**) and a better clearance (Kep) (**B**) in metoprolol-treated rats. These changes led to a reduction in the extracellular volume (ECV) in rats receiving metoprolol (Ktrans:Kep), thus suggesting a preservation of the BBB (see Figure 4) (vehicle, n = 5; metoprolol, n = 10). Graphs show mean \pm S.E.M; unpaired Mann-Whitney or Student t-test.



Supplemental Figure 6. Representative IgG immunohistochemistry (IHC) on coronal sections at 7 d post-reperfusion, showing IgG extravasation in the core lesion of a vehicle-treated rat (upper panels) and its absence in a metoprolol-treated one (lower panels). IgG extravasation in the basal ganglia (outlined in purple) at 7 d post-reperfusion was attenuated in metoprolol-treated rats.



Supplemental Figure 7. (A) Representative IHC of NeuN, GFAP and Iba1 on coronal sections at 24 h post-reperfusion, showing no changes in the core lesion between vehicle (left) and metoprolol (right). Neuronal nuclei lost staining and microglia started to acquire a reactive morphology; however, early after reperfusion, there is not glial scarring yet, nor microglia/macrophages pro-inflammatory response and accumulation. (B) Representative IHC of aquaporin 4 (AQP4) on coronal sections at 24 h postreperfusion, which show no changes in the core lesion between vehicle (top row) and metoprolol (bottom row). Quantification of AQP4 IHC in the MCA of infarcted hemispheres shows no differences between both treatments. Vehicle, n=5; metoprolol, n=7. Graphs show mean \pm S.E.M; unpaired Student t-test.



Supplemental Figure 8. (A) Representative GFAP immunohistochemistry (IHC) on coronal sections at 7 d post-reperfusion, showing a glial scar (red outline) in the core lesion of a vehicle-treated rat (left) and the absence of scarring in a metoprolol-treated rat (right). Glial scar size was measured as the area lacking astrocytes in the middle cerebral artery (MCA) territory (outlined in orange) at 7 d post-reperfusion, showing abolition of scarring in metoprolol-treated rats. (B) Representative IHC of chondroitin sulfate proteoglycans (CSPGs) on coronal sections at 7 d post-reperfusion, showing CSPG deposition (red outline) in the core lesion of a vehicle-treated rat (left) and its absence in a metoprolol-treated rat (right). CSPG deposition in the basal ganglia (outlined in purple) at 7 d post-reperfusion was attenuated in metoprolol-treated rats. (C) Representative myelin basic protein (MBP) IHC on coronal sections at 7 d post-reperfusion, showing myelin sheath degeneration in the core lesion (red outline) of a vehicle-treated rat (left) and preserved myelination in a metoprolol-treated rat (right). Quantification of basal ganglia (outlined in purple) myelin sheath degeneration at 7 d post-reperfusion shows preserved myelination in metoprolol-treated rats. High magnification views illustrate this process. (D) Representative double immunostaining for CSPG (blue) and GFAP (brown), showing a glial scar filled with a proteoglycan matrix in a vehicle-treated rat (left) and the absence of scarring in a metoprolol-treated rat (right). (E) Representative double immunostaining for CSPG (blue) and MBP (brown), showing CSPG deposition and the accumulation of myelin sheath debris in the core lesion of a vehicle-treated rat, creating an inhibitory context for axonal and neuronal regeneration. In the metoprolol-injected rat, CSPG deposition is inhibited and myelin sheaths are preserved.

**DECLARACIÓN JURADA DE AUTORÍA DEL TRABAJO
CIENTÍFICO,
PARA LA DEFENSA DEL TRABAJO FIN DE MASTER**

Fecha: 03/06/2023

Quien suscribe:

Autor(a): Agustín Clemente Moragón
D.N.I./N.I.E./Pasaporte.: 50236389L

Hace constar que es el autor(a) del trabajo:

"Evaluation of brain ischemia/reperfusion injury and the impact of new neuroprotective strategies using Magnetic Resonance Imaging"

En tal sentido, manifiesto la originalidad de la conceptualización del trabajo, interpretación de datos y elaboración de las conclusiones, dejando establecido que aquellos aportes intelectuales de otros autores, se han referenciado debidamente en el documento que se entrega.

DECLARACIÓN:

- ✓ Garantizo que el trabajo que remito es un documento original y no ha sido publicado, total ni parcialmente por otros autores, en soporte papel ni en formato digital.
- ✓ Certifico que he contribuido directamente al contenido intelectual de este manuscrito, a la génesis y análisis de sus datos, por lo cual estoy en condiciones de hacerme públicamente responsable de él.
- ✓ No he incurrido en fraude científico, plagio o vicios de autoría; en caso contrario, aceptaré las medidas disciplinarias sancionadoras que correspondan.

Fdo. **CLEMENTE MORAGON AGUSTIN** - 50236389L
56 **50236389L**

Firmado digitalmente por
CLEMENTE MORAGON AGUSTIN
- 50236389L
Fecha: 2023.06.03
17:09:20 +02'00'